Integral Line-of-Sight Guidance for Path Following Control of Underwater Snake Robots: Theory and Experiments

Eleni Kelasidi, *Member, IEEE,* Pål Liljebäck, *Member, IEEE,* Kristin Y. Pettersen, *Senior Member, IEEE,* and Jan Tommy Gravdahl, *Senior Member, IEEE*

Abstract—This paper proposes and experimentally validates a straight line path following controller for underwater snake robots in the presence of constant irrotational currents of unknown direction and magnitude. An integral line-of-sight (LOS) guidance law is presented, which is combined with a sinusoidal gait pattern and a directional controller that steers the robot towards and along the desired path. The stability of the proposed control scheme in the presence of ocean currents is investigated by using Poincaré map analysis. Simulation results are presented to illustrate the performance of the proposed path following controller for both lateral undulation and eel-like motion. In addition, the performance of the path following controller is investigated through experiments with a physical underwater snake robot. The experimental results show that the proposed control strategy successfully steers the robot towards and along the desired path in the presence of an unknown constant irrotational current in the inertial frame.

Index Terms—Underwater snake robots, modeling of swimming robots, path following controller, integral LOS.

I. INTRODUCTION

FOR centuries, engineers and scientists have gained inspiration from the natural world in their search for solutions to technical problems, and this process is termed biomimetics. Underwater snake robots have several promising applications for underwater exploration, monitoring, surveillance and inspection. They thus bring a promising prospective to improve the efficiency and maneuverability of modern-day underwater vehicles. For instance, these mechanisms carry a lot of potential for inspection of subsea oil and gas installations. Also, for the biological community and marine archeology, snake robots that are able to swim smoothly without much noise, and that can navigate in difficult environments such as ship wrecks, are very interesting [1]. To realize operational snake robots for such underwater applications, a number of different control design challenges must first be solved. An important control problem concerns the ability to follow given reference paths under the influence of ocean current effects, and this is the topic of this paper.

Based on the dynamic model presented in [1], [2], we propose an integral line-of-sight path following controller for steering an underwater snake robot along a straight line

E. Kelasidi, P. Liljebäck and K. Y. Pettersen are with the Centre for Autonomous Marine Operations and Systems, Dept. of Engineering Cybernetics at NTNU, NO-7491 Trondheim, Norway. E-mail: {Eleni.Kelasidi,Pal.Liljeback,Kristin.Y.Pettersen}@itk.ntnu.no

J. T. Gravdahl is with the Dept. of Engineering Cybernetics at NTNU, NO-7491 Trondheim, Norway. E-mail: Tommy.Gravdahl@itk.ntnu.no

path in the presence of ocean currents of unknown direction and magnitude. Unlike the biologically inspired flow sensing strategy presented in [3], the integral LOS guidance law proposed in this paper is inspired by path following control of marine surface vessels in the presence of ocean currents [4], [5]. Note that the integral LOS guidance strategy is widely used for directional control of marine surface vessels for ocean current compensation but has not been employed previously for directional control of underwater snake robots in the presence of ocean currents. Preliminary results of the proposed control strategy are also presented in [2], but whereas the efficacy of the control strategy is supported by simulation results in [2], this paper investigates the efficacy of the integral LOS path following control strategy through experiments with a physical underwater snake robot [6]. The experimental results show that the integral LOS guidance law can be applied to underwater snake robots to compensate for the ocean drift effects, including the current effects, and achieve path following of straight lines. Experimental results for path following of a 5 links underwater snake robot and a fish robot have been presented in [7] and [8], respectively. However, to the authors' best knowledge, experimental results for path following control of underwater snake robots compensating for the current effects have not been investigated in previous literature.

Furthermore, motivated by [9], [10], the stability of the locomotion of an underwater snake robot along the straight line path in the presence of ocean currents using a Poincaré map is analyzed. The method of Poincaré maps is a widely used tool for studying the stability of periodic solutions in dynamical systems. In particular, by using a Poincaré map, we prove that all state variables of an underwater snake robot, except the position along the forward direction, trace out an exponentially stable periodic orbit when the integral LOS path following controller is applied. As far as we know, no formal stability analysis of an integral LOS path following controller for an underwater snake robot has been presented in previous literature.

The paper is organized as follows. Section II presents a research background on swimming robots. Section III presents the dynamic model of an underwater snake robot, while the integral line-of-sight path following controller along straight lines is outlined in Section IV. The stability analysis based on the Poincaré map approach is presented in Section V, followed by simulation results for both lateral undulation and eel-like motion in Section VI. Experimental results are presented in Section VII. Finally, conclusions and suggestions for further research are given in Section VIII.

II. BACKGROUND ON BIOLOGICALLY INSPIRED SWIMMING ROBOTS

Studies of biologically inspired snake robots have largely restricted themselves to land-based studies for which reviews on modelling, implementation, and control of snake robots can be found in [11], [12]. Empirical and analytic studies of snake locomotion were reported by [13], while the work of [14] is among the first approaches to develop a snake robot prototype. Several land-based snake robots [15]–[19] and biologically inspired swimming robots [3], [6], [8], [20]–[32] have been constructed since then. Comparing amphibious snake robots to the traditional land-based ones, the former have the advantage of adaptability to aquatic environments. The research activity on amphibious snake robots (also referred to as lamprey or eel-like robots) that can operate in aquatic environments, is less extensive. Due to the complex dynamics of swimming snake robots, several different modeling approaches have been carried out in the literature [1], [7], [24], [33]–[42]. Several results have been reported in the related field of design, modeling and control of underwater robots that mimic the movement of fish [3], [8], [30], [43]–[47]. In addition, physical sea snakes has been studied by University of Adelaide researchers as inspiration for an underwater robot design [48]. Regarding swimming snake robots, the underlying propulsive force generation mechanism has been studied through exploration of the fluid dynamics surrounding the body [36].

Classical works by Taylor [33] and Lighthill [34] provide analytic models of fluid forces acting on the body during undulatory swimming. McIsaac and Ostrowski [7] present a dynamic model of anguilliform swimming for eel-like robots and Boyer et al. [35] present the dynamic modeling of a continuous three-dimensional swimming eel-like robot. Chen et al. [36] demonstrate a model for the body-fluid interaction in undulatory swimming of leeches, where the body is represented by a chain of rigid links and the hydrodynamic force model is based on resistive and reactive force theories. [38] presents the equations of motion for a general multibody rectifier system taking into account the currents by assuming that the environmental force is a (possibly nonlinear) function of the relative velocity (i.e. the velocity of the link in water in the presence of current). However, the added mass and the fluid torque effects (also referred to as fluid moments) are not taken into account (for more details, see [1]). [39] presents the modeling of the reactive force and moment acting on an elongated body moving in a weakly non-uniform potential flow. This model has been used to investigate the passive and the active swimming of a fish in a vortex street. In [49], a solution to the fast dynamics of eel-like robots has been proposed and tested in comparison with a Navier-Stokes solver. In [24], the dynamic model of a fish-like robot named AmphiBot III is presented. This modeling approach is based on the adaptation of Lighthill's large amplitude elongated body theory to a serial mobile multibody system and the results are compared to the planar motion of the real robot for forward swimming gaits and turning maneuvers.

The majority of the modeling results for underwater robots omit fluid moments (fluid torques) which are then assumed to have a negligible effect on the overall motion of the system [7], [38], [50]. However, the fluid torques are directly related to the power consumption of the system (see e.g. [37]), and it is thus interesting to include them in order to achieve a more accurate modeling approach from a hydro-dynamic perspective and energy efficient motion. In [35], [37] and [51] fluid torques are modeled, but the drag force and torque are integrated numerically at each sample time of the algorithm and evaluated numerically, something which results in the lack of a closed form solution. For control design purposes, it is a main advantage that the hydrodynamic modeling concludes in a closed form, without the need of an algorithmic way to compute the drag force and torque. Furthermore, in [40], a simplified model of [38] is used to develop a feedback controller that achieves the desired body oscillation, orientation, and locomotion velocity. In [52], a solution to the modeling problem that results in a closed form solution is presented. This approach considers hydrodynamic and hydrostatic forces and torques and avoids the numerical evaluation of drag effects. The modeling approach in [1], [2] considers both linear and nonlinear drag forces (resistive fluid forces), the added mass effect (reactive fluid forces), the fluid moments and current effect. Note that as far as the fluid effects are considered, for control design purposes, in [1], [2] the hydrodynamic phenomena are modeled in a sufficiently simple manner while taking into account all the hydrodynamic effects that are significant for the control design. Furthermore in [52], hydrostatic forces (gravitational and buoyancy forces) are considered, under the assumption that these forces are coincident. This modeling approach combines the hydrodynamic effects, as derived in [1], in analytical-closed form with the hydrostatic forces. Note that the model presented in [1], [2] is in closed-loop form and is thus particularly well suited for modern model-based control design schemes. The control design in this paper, will thus be based on the model presented in [1], [2].

Several control approaches for underwater snake robots have been proposed in the literature. However, the emphasis so far has mainly been on achieving forward and turning locomotion [24], [53]. The next step would be not only to achieve forward locomotion, but also to make the snake robot follow a desired path, i.e. solving the path following control problem. The works of [7], [54] and [8] synthesize gaits for translational and rotational motion of various fish-like mechanisms and propose controllers for tracking straight and curved trajectories. The work of [23] studies the evolution from fish to amphibian by use of central pattern generators (CPG). Eel-like motion is considered in [7] and [55], where controllers for tracking straight and curved trajectories are proposed. [56] proposes a solution for steering an underwater snake robot along a path, defined by straight lines of interconnected points that combines the use of an artificial potential fields-based path planner with a new waypoint guidance strategy for an underwater snake robot, but no formal proof is presented. Another waypoint guidance strategy, where the waypoints are defined a priori, is proposed for a Carangiform swimmer in [57]. A solution to the obstacle avoidance problem of an electric fish-like robot is presented in [58]. However, path following control for underwater snake robots still remains an open problem.

In [59], results of a feedback control scheme for 3D movement of the robot's continuous model in [35] are presented. The stabilization of the rolling angle is achieved with two pectoral fins that are attached to the head of the robot. In [60], motion control of a three-dimensional eel-like robot without pectoral fins is presented. This controller enables the tracking of a desired 3D position of the eel head as well as the stabilization of the rolling angle without pectoral

fins. A multi-variable constrained feedback control scheme is proposed in [61] based on a reduced model of an eel robot. [62] presents a solution for path following of eel-like robots where a type of autonomous gait generation is developed by explicitly controlling the local system curvature. The proposed path following controller is inspired by the one of marine vehicles and the heading control is combined with the *virtual target* principle. Experimental validation of open-loop motion planning for eel-like robot is presented in [7], [24], [53]. In addition, [7] presents closed-loop experiments for straight-line tracking and disturbance rejection in the plane, using image-based position feedback. These preliminary closed-loop experiments with eel-like robot proved the concept, but were not satisfactory for closed-loop control, as mentioned by the authors [7]. In [63] simulation and experimental results have been presented based on the line-of-sight guidance law for steering an underwater snake robot along a straight line path. However, all these previous approaches for path following control are based on dynamic models of the swimming robots where ocean current effects are neglected.

Biological swimming animals as well as underwater swimming robots operate under the influence of highly nonlinear hydrodynamic effects, e.g. turbulent fluid, current and wave effects [3]. The key to successfully manoeuvring under complex hydrodynamic effects for aquatic animals lies in the ability to sense, process and react to environmental disturbances. Fish and aquatic organisms may actively orient either positively (upstream/positive rheotaxis) to minimize the drag or negatively (downstream/negative rheotaxis) to water flows [64]. Rheotaxis, i.e. orientation to currents, is a robust, multisensory behavior found in many aquatic organisms. Biological fish have a lateral line sensing organ in order to detect movement and vibration in the surrounding water, providing spatial awareness and the ability to navigate in space [64]. Biological studies of aquatic animals show that lateral line is important in many behaviors, including rheotaxis, prey detection, predator avoidance, station holding, spawning behavior and schooling behavior [3], [65]. Flow sensing is used in [3] to control a fish robot. A flow-aided path following control strategy for fish robots is presented in [3], [46]. From experimental results, it is shown that the fish robot manages to follow the desired trajectory in the flow by adjusting its flow-relative speed and using the side-slipping effect. In this paper, however, we develop a controller that is able to compensate for the current effects in the absence of sensing the surrounding flow effects. In particular, the proposed control approach does not need any sensors measuring the surrounding flow effects. The only measurements needed are the position and orientation of the robot.

III. MATHEMATICAL MODEL OF UNDERWATER SNAKE ROBOT

This section briefly presents the model of the kinematics and dynamics of an underwater snake robot moving in a virtual horizontal plane that will be used in the control design and analysis of this paper. A more detailed presentation of the model is given in [1], [2].

A. Notations and Defined Symbols

The underwater snake robot consists of n rigid links of equal length $2l$ interconnected by $n-1$ joints. The links are assumed
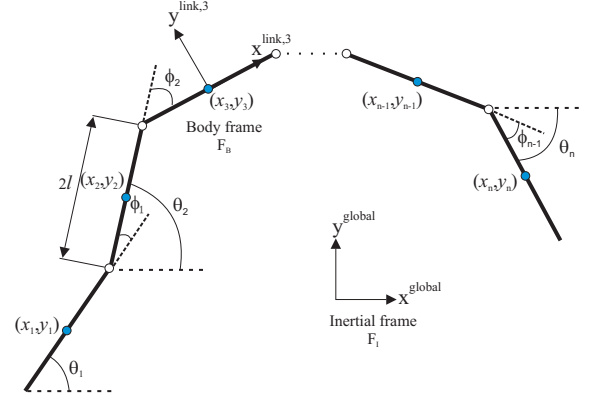

Fig. 1. Kinematic parameters of the underwater snake robot.

to have the same mass m and moment of inertia $J = \frac{1}{3}ml^2$. The mass of each link is uniformly distributed so that the link CM (center of mass) is located at its center point (at length l from the joint at each side). The total mass of the snake robot is therefore nm. In the following subsections, the kinematics and dynamics of the robot will be described in terms of the mathematical symbols described in Table I and illustrated in Fig. 1 and Fig. 2. The following vectors and matrices are used in the subsequent sections:

$$\mathbf{A} = \begin{bmatrix} 1 & 1 & & \\ & \ddots & \ddots & \\ & & 1 & 1 \end{bmatrix}, \mathbf{D} = \begin{bmatrix} 1 & -1 & & \\ & \ddots & \ddots & \\ & & 1 & -1 \end{bmatrix},$$

where $\mathbf{A}, \mathbf{D} \in \mathbb{R}^{(n-1) \times n}$. Furthermore,

$$\mathbf{e} = \begin{bmatrix} 1 & \dots & 1 \end{bmatrix}^T \in \mathbb{R}^n, \mathbf{E} = \begin{bmatrix} \mathbf{e} & \mathbf{0}_{n \times 1} \\ \mathbf{0}_{n \times 1} & \mathbf{e} \end{bmatrix} \in \mathbb{R}^{2n \times 2},$$

$$\begin{aligned}
\sin \boldsymbol{\theta} &= \begin{bmatrix} \sin \theta_1 & \dots & \sin \theta_n \end{bmatrix}^T \in \mathbb{R}^n, \\
\mathbf{S}_\theta &= \operatorname{diag}(\sin \boldsymbol{\theta}) \in \mathbb{R}^{n \times n}, \\
\cos \boldsymbol{\theta} &= \begin{bmatrix} \cos \theta_1 & \dots & \cos \theta_n \end{bmatrix}^T \in \mathbb{R}^n, \\
\mathbf{C}_\theta &= \operatorname{diag}(\cos \boldsymbol{\theta}) \in \mathbb{R}^{n \times n}, \\
\operatorname{sgn}\boldsymbol{\theta} &= \begin{bmatrix} \operatorname{sgn}\theta_1 & \dots & \operatorname{sgn}\theta_n \end{bmatrix}^T \in \mathbb{R}^n \\
\dot{\boldsymbol{\theta}}^2 &= \begin{bmatrix} \dot{\theta}_1^2 & \dots & \dot{\theta}_n^2 \end{bmatrix}^T \in \mathbb{R}^n, \mathbf{J} = J\mathbf{I}_n, \mathbf{L} = l\mathbf{I}_n
\end{aligned}$$

$$\mathbf{M} = m\mathbf{I}_n, \mathbf{K} = \mathbf{A}^T \left(\mathbf{D}\mathbf{D}^T\right)^{-1} \mathbf{D}, \mathbf{V} = \mathbf{A}^T \left(\mathbf{D}\mathbf{D}^T\right)^{-1} \mathbf{A}$$

The matrices $\mathbf{A}$ and $\mathbf{D}$ represent, respectively, an addition and a difference matrix, which will be used, for adding and subtracting pairs of adjacent elements of a vector. Furthermore, the vector $\mathbf{e}$ represents a summation vector, which is used for adding all elements of a n-dimensional vector.

B. Kinematics of Underwater Snake Robot

The snake robot is assumed to move in a virtual horizontal plane, fully immersed in water, and has $n+2$ degrees of freedom (n links angles and the x-y position of the robot). The *link angle* of each link $i \in 1, \dots, n$ of the snake robot is denoted by $\theta_i \in \mathbb{R}$, while the *joint angle* of joint $i \in 1, \dots, n-1$ is given by $\phi_i = \theta_i - \theta_{i-1}$. The link angles and the joint angles
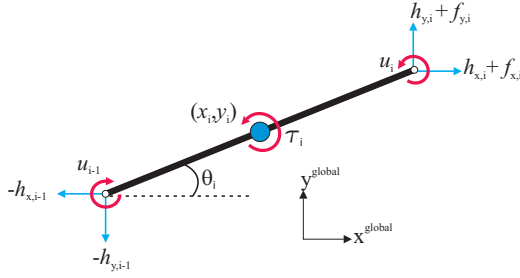
Fig. 2. Forces and torques acting on each link of the underwater snake robot.

TABLE I
DEFINITION OF MATHEMATICAL TERMS

Symbol	Description	Vector
n	The number of links	
l	The half length of a link	
m	Mass of each link	
J	Moment of inertia of each link	
θ_i	Angle between link i and the global x axis	$\boldsymbol{\theta} \in \mathbb{R}^n$
ϕ_i	Angle of joint i	$\boldsymbol{\phi} \in \mathbb{R}^{n-1}$
(x_i, y_i)	Global coordinates of the CM of link i	$\mathbf{X}, \mathbf{Y} \in \mathbb{R}^n$
(p_x, p_y)	Global coordinates of the CM of the robot	$\mathbf{p}_{\text{CM}} \in \mathbb{R}^2$
u_i	Actuator torque of joint between link i and link $i+1$	$\mathbf{u} \in \mathbb{R}^{n-1}$
u_{i-1}	Actuator torque of joint between link i and link $i-1$	$\mathbf{u} \in \mathbb{R}^{n-1}$
$f_{x,i}$	Fluid force on link i in x direction	$\mathbf{f_x} \in \mathbb{R}^n$
$f_{y,i}$	Fluid force on link i in y direction	$\mathbf{f_y} \in \mathbb{R}^n$
τ_i	Fluid torque on link i	$\boldsymbol{\tau} \in \mathbb{R}^n$
$h_{x,i}$	Joint constraint force in x direction on link i from link $i+1$	$\mathbf{h_x} \in \mathbb{R}^{n-1}$
$h_{y,i}$	Joint constraint force in y direction on link i from link $i+1$	$\mathbf{h_y} \in \mathbb{R}^{n-1}$
$h_{x,i-1}$	Joint constraint force in x direction on link i from link $i-1$	$\mathbf{h_x} \in \mathbb{R}^{n-1}$
$h_{y,i-1}$	Joint constraint force in y direction on link i from link $i-1$	$\mathbf{h_y} \in \mathbb{R}^{n-1}$

are assembled in the vectors $\boldsymbol{\theta} = [\theta_1, \ldots, \theta_n]^T \in \mathbb{R}^n$ and $\boldsymbol{\phi} = [\phi_1, \ldots, \phi_{n-1}]^T \in \mathbb{R}^{n-1}$, respectively. The *heading* (or *orientation*) $\bar{\theta} \in \mathbb{R}$ of the snake is defined as the average of the link angles, i.e. as [9]

$$\bar{\theta} = \frac{1}{n} \sum_{i=1}^{n} \theta_i. \qquad (1)$$

The global frame position $\mathbf{p}_{\text{CM}} \in \mathbb{R}^2$ of the CM (center of mass) of the robot is given by

$$\mathbf{p}_{\text{CM}} = \begin{bmatrix} p_x \\ p_y \end{bmatrix} = \begin{bmatrix} \frac{1}{nm} \sum_{i=1}^{n} m x_i \\ \frac{1}{nm} \sum_{i=1}^{n} m y_i \end{bmatrix} = \frac{1}{n} \begin{bmatrix} \mathbf{e}^T \mathbf{X} \\ \mathbf{e}^T \mathbf{Y} \end{bmatrix}, \quad (2)$$

where (x_i, y_i) are the global frame coordinates of the CM of link i, $\mathbf{X} = [x_1, \ldots, x_n]^T \in \mathbb{R}^n$ and $\mathbf{Y} = [y_1, \ldots, y_n]^T \in \mathbb{R}^n$. The forward velocity of the robot is denoted by $\bar{v}_t \in \mathbb{R}$ and is defined as the component of the CM velocity along the current heading of the snake, i.e.

$$\bar{v}_t = \dot{p}_x \cos \bar{\theta} + \dot{p}_y \sin \bar{\theta}. \qquad (3)$$

C. Hydrodynamic Modeling

As it has been noted in the bio-robotics community, underwater snake (eel-like) robots bring a promising prospective to improve the efficiency and maneuverability of modern-day underwater vehicles. The dynamic modeling of the contact forces is, however, quite complicated compared to the modeling of the overall rigid motion. The Navier-Stokes equations are very difficult to solve and quite unsuited for robotics control design purposes. The hydrodynamic modeling approach from [1] that is considered in this paper, takes into account both the linear and the nonlinear drag forces (resistive fluid forces), the added mass effect (reactive fluid forces), the fluid moments and current effects.

1) Model assumptions: underlying the modeling approach.

Assumption 1. The fluid is viscid, incompressible, and irrotational in the inertia frame.

Assumption 2. The robot is neutrally buoyant, i.e, we assume that the mass per unit of volume of the robot is equal to that of the water, such that gravity and buoyancy cancel each other out.

Assumption 3. The current in the inertial frame, $v_c = [V_{x,i}, V_{y,i}]^T$, is constant and irrotational.

Remark 1. Assumptions 1 and 2 are common assumptions in hydrodynamic modeling of slender body swimming robots [35], [37], while Assumption 3 is a reasonable simplification of the real-world situation and is a standard assumption in marine control theory [66], [67].

Remark 2. Neutral buoyancy, ensuring that Assumption 2 is satisfied, is achieved by proper ballasting of the snake robot. The ballast will furthermore be positioned at the bottom of each snake robot link, in order to prevent it from rolling, making it self-stabilized in roll.

Assumption 4. The relative velocity at each point of the link in body-fixed frame (F_B) is equal to the relative velocity of the respective center of mass of each link.

Remark 3. This approximation is valid in our case because the link's length is small compared to the total robot's length, which means that the linear velocity of each point along a link will be approximately the same. With this assumption, we avoid the complexity of deriving the drag forces in analytical form, due to the nonlinear terms.

2) Hydrodynamic model: In [1], it is shown that the fluid forces on all links can be expressed in vector form as

$$\mathbf{f} = \begin{bmatrix} \mathbf{f_x} \\ \mathbf{f_y} \end{bmatrix} = \begin{bmatrix} \mathbf{f}_{\mathbf{A_x}} \\ \mathbf{f}_{\mathbf{A_y}} \end{bmatrix} + \begin{bmatrix} \mathbf{f}_{\mathbf{D_x}}^{\mathrm{I}} \\ \mathbf{f}_{\mathbf{D_y}}^{\mathrm{I}} \end{bmatrix} + \begin{bmatrix} \mathbf{f}_{\mathbf{D_x}}^{\mathrm{II}} \\ \mathbf{f}_{\mathbf{D_y}}^{\mathrm{II}} \end{bmatrix}. \qquad (4)$$

The vectors $\mathbf{f}_{\mathbf{A_x}}$ and $\mathbf{f}_{\mathbf{A_y}}$ represent the effects from added mass forces and are expressed as

$$\begin{bmatrix} \mathbf{f}_{\mathbf{A_x}} \\ \mathbf{f}_{\mathbf{A_y}} \end{bmatrix} = - \begin{bmatrix} \mu_n (\mathbf{S}_\theta)^2 & -\mu_n \mathbf{S}_\theta \mathbf{C}_\theta \\ -\mu_n \mathbf{S}_\theta \mathbf{C}_\theta & \mu_n (\mathbf{C}_\theta)^2 \end{bmatrix} \begin{bmatrix} \ddot{\mathbf{X}} \\ \ddot{\mathbf{Y}} \end{bmatrix}$$
$$- \begin{bmatrix} -\mu_n \mathbf{S}_\theta \mathbf{C}_\theta & -\mu_n (\mathbf{S}_\theta)^2 \\ \mu_n (\mathbf{C}_\theta)^2 & \mu_n \mathbf{S}_\theta \mathbf{C}_\theta \end{bmatrix} \begin{bmatrix} \mathbf{V}_x^a \\ \mathbf{V}_y^a \end{bmatrix} \dot{\boldsymbol{\theta}}, \qquad (5)$$

where $\mathbf{V}_x^a = \text{diag}(V_{x,1}, \ldots, V_{x,n}) \in \mathbb{R}^{n \times n}$, $\mathbf{V}_y^a = \text{diag}(V_{y,1}, \ldots, V_{y,n}) \in \mathbb{R}^{n \times n}$ and $[V_{x,i}, V_{y,i}]^T$ is the current velocity expressed in inertial frame coordinates. The drag forces on the robot are given by

$$\begin{bmatrix} \mathbf{f}_{\mathbf{D_x}}^{\mathrm{I}} \\ \mathbf{f}_{\mathbf{D_y}}^{\mathrm{I}} \end{bmatrix} = - \begin{bmatrix} c_t \mathbf{C}_\theta & -c_n \mathbf{S}_\theta \\ c_t \mathbf{S}_\theta & c_n \mathbf{C}_\theta \end{bmatrix} \begin{bmatrix} \mathbf{V}_{\mathbf{r_x}} \\ \mathbf{V}_{\mathbf{r_y}} \end{bmatrix}, \qquad (6)$$

$$\left[\begin{array}{c} \mathbf{f}_{\mathbf{D_x}}^{\mathrm{II}} \\ \mathbf{f}_{\mathbf{D_y}}^{\mathrm{II}} \end{array} \right] = - \left[\begin{array}{cc} c_t \mathbf{C}_\theta & -c_n \mathbf{S}_\theta \\ c_t \mathbf{S}_\theta & c_n \mathbf{C}_\theta \end{array} \right] \mathrm{sgn}\left(\left[\begin{array}{c} \mathbf{V}_{\mathbf{r_x}} \\ \mathbf{V}_{\mathbf{r_y}} \end{array} \right] \right) \left[\begin{array}{c} \mathbf{V}_{\mathbf{r_x}}{}^2 \\ \mathbf{V}_{\mathbf{r_y}}{}^2 \end{array} \right],$$

$$(7)$$

where $\mathbf{f}_{\mathbf{D_x}}^{\mathrm{I}}$, $\mathbf{f}_{\mathbf{D_y}}^{\mathrm{I}}$ and $\mathbf{f}_{\mathbf{D_x}}^{\mathrm{II}}$, $\mathbf{f}_{\mathbf{D_y}}^{\mathrm{II}}$ are the linear and nonlinear drag, respectively, and where the relative velocities are given by

$$\left[\begin{array}{c} \mathbf{V}_{\mathbf{r_x}} \\ \mathbf{V}_{\mathbf{r_y}} \end{array} \right] = \left[\begin{array}{cc} \mathbf{C}_\theta & \mathbf{S}_\theta \\ -\mathbf{S}_\theta & \mathbf{C}_\theta \end{array} \right] \left[\begin{array}{c} \dot{\mathbf{X}} - \mathbf{V}_x \\ \dot{\mathbf{Y}} - \mathbf{V}_y \end{array} \right]. \qquad (8)$$

In addition, the fluid torques on all links are

$$\boldsymbol{\tau} = -\boldsymbol{\Lambda}_1 \ddot{\boldsymbol{\theta}} - \boldsymbol{\Lambda}_2 \dot{\boldsymbol{\theta}} - \boldsymbol{\Lambda}_3 \dot{\boldsymbol{\theta}} |\dot{\boldsymbol{\theta}}|, \qquad (9)$$

where $\boldsymbol{\Lambda}_1 = \lambda_1 \mathbf{I}_n$, $\boldsymbol{\Lambda}_2 = \lambda_2 \mathbf{I}_n$ and $\boldsymbol{\Lambda}_3 = \lambda_3 \mathbf{I}_n$. The coefficients c_t, c_n, λ_2, λ_3 represent the drag forces parameters due to the pressure difference between the two sides of the body, and the parameters μ_n, λ_1 represent the added mass of the fluid carried by the moving body. Note that the added mass parameter in the x direction is considered equal to zero ($\mu_t = 0$), because the added mass of a slender body in the longitudinal direction can be neglected compared to the body mass [1].

D. Equations of Motion

This section presents the equations of motion for the underwater snake robot. In [1], [2] it is shown that the acceleration of the CM may be expressed as

$$\left[\begin{array}{c} \ddot{p}_x \\ \ddot{p}_y \end{array} \right] = -\mathbf{M}_p \left[\begin{array}{cc} \mathbf{k}_{11} & \mathbf{k}_{12} \\ \mathbf{k}_{21} & \mathbf{k}_{22} \end{array} \right] \left[\begin{array}{c} l\mathbf{K}^T(\mathbf{C}_\theta \dot{\boldsymbol{\theta}}^2 + \mathbf{S}_\theta \ddot{\boldsymbol{\theta}}) \\ l\mathbf{K}^T(\mathbf{S}_\theta \dot{\boldsymbol{\theta}}^2 - \mathbf{C}_\theta \ddot{\boldsymbol{\theta}}) \end{array} \right]$$
$$- \mathbf{M}_p \left[\begin{array}{cc} \mathbf{k}_{12} & -\mathbf{k}_{11} \\ \mathbf{k}_{22} & -\mathbf{k}_{21} \end{array} \right] \left[\begin{array}{c} \mathbf{V}_x^a \\ \mathbf{V}_y^a \end{array} \right] \dot{\boldsymbol{\theta}} + \mathbf{M}_p \left[\begin{array}{c} \mathbf{e}^T \mathbf{f}_{\mathbf{Dx}} \\ \mathbf{e}^T \mathbf{f}_{\mathbf{Dy}} \end{array} \right],$$

$$(10)$$

where the detailed derivation of the matrix $\mathbf{M}_p$ and vectors $\mathbf{k}_{11}$, $\mathbf{k}_{12}$, $\mathbf{k}_{21}$ and $\mathbf{k}_{22}$ is given in [2]. In addition, it is shown that under the influence of fluid forces (4) and torques (9), the complete equation of motion of the underwater snake robot are obtained by (10) and

$$\mathbf{M}_\theta \ddot{\boldsymbol{\theta}} + \mathbf{W}_\theta \dot{\boldsymbol{\theta}}^2 + \mathbf{V}_\theta \dot{\boldsymbol{\theta}} + \boldsymbol{\Lambda}_3 |\dot{\boldsymbol{\theta}}|\dot{\boldsymbol{\theta}} + \mathbf{K_{Dx}} \mathbf{f_{Dx}} + \mathbf{K_{Dy}} \mathbf{f_{Dy}} = \mathbf{D}^T \mathbf{u},$$
$$(11)$$

with $\mathbf{f_{Dx}} = \mathbf{f}_{\mathbf{D_x}}^{\mathrm{I}} + \mathbf{f}_{\mathbf{D_x}}^{\mathrm{II}}$ and $\mathbf{f_{Dy}} = \mathbf{f}_{\mathbf{D_y}}^{\mathrm{I}} + \mathbf{f}_{\mathbf{D_y}}^{\mathrm{II}}$ representing the drag forces in x and y directions and $\mathbf{u} \in \mathbb{R}^{n-1}$ the control input. For more details and the derivation of the matrices $\mathbf{M}_\theta$, $\mathbf{W}_\theta$, $\mathbf{V}_\theta$, $\mathbf{K_{Dx}}$ and $\mathbf{K_{Dy}}$, see [2].

By introducing the state vector $\mathbf{x_s} = \left[\boldsymbol{\theta}^T, \mathbf{p}_{\mathrm{CM}}^T, \dot{\boldsymbol{\theta}}^T, \dot{\mathbf{p}}_{\mathrm{CM}}^T \right]^T \in \mathbb{R}^{2n+4}$, we can rewrite the model of the robot compactly in state space form as

$$\dot{\mathbf{x}}_\mathbf{s} = \left[\dot{\boldsymbol{\theta}}^T, \dot{\mathbf{p}}_{\mathrm{CM}}^T, \ddot{\boldsymbol{\theta}}^T, \ddot{\mathbf{p}}_{\mathrm{CM}}^T \right]^T = \mathbf{F}(\mathbf{x_s}, \mathbf{u}) \qquad (12)$$

where the elements of $\mathbf{F}(\mathbf{x_s}, \mathbf{u})$ are found by solving (10) and (11) for $\ddot{\mathbf{p}}_{\mathrm{CM}}$ and $\ddot{\boldsymbol{\theta}}$, respectively.

E. Discussion

Although the model of an underwater snake robot presented in this paper is in closed form and is thus better suited for modern model-based control design schemes than models that involves numerical calculations, this model considered underwater snake robots swimming in a horizontal 2D plane of 3D. Consequently, based on this model, we are able to investigate problems regarding the motion of swimming robots with highly nonlinear and complex models in 2D space, as a preliminary step before we target more complicated problems in the three-dimensional space. Many interesting applications of underwater snake robots demands motion in 3D plane, and even though motion in any tilted horizontal plane will cover several of these applications, it is natural to extend the modeling approach presented in this paper from 2D to 3D in future work.

In addition, it is interesting to note that if, in the dynamic model (10) and (11), we set the fluid parameters to zero and replace the drag forces in x and y direction with ground friction models, then the model reduces exactly to the dynamic model of a ground snake robot described in [9]. The underwater snake robot model is thus an extension of the land snake robot model, and may be used for amphibious snake robots moving both on land and in water.

IV. INTEGRAL LOS PATH FOLLOWING CONTROL

In this section we propose an integral LOS path following control scheme for underwater snake robots [2]. The controller consists of three main components as shown in Fig. 3. The first component is the gait pattern controller, which produces a sinusoidal motion pattern which propels the robot forward. The second component is the heading controller, which steers the robot towards and subsequently along the desired path. The third component is the integral LOS guidance law (Fig. 4), which generates the desired heading angle in order to follow the desired path. An inner loop PD controller is used to control the joint angles ϕ, while an outer loop controller is used for generating the reference joint angles in order to achieve the desired sinusoidal gait pattern and also the desired heading $\bar{\theta}_{\mathrm{ref}}$ (Fig. 3). The three components of the path following controller will be presented in the following subsections.

A. Control Objective

The path following control objective is to make the robot converge to the desired straight line path and subsequently progress along the path at some nonzero forward velocity $\bar{v}_t > 0$, where $\bar{v}_t$ is defined in (3). We consider it as less important to accurately control the forward velocity of the robot since in [68], [69] based on both extensive simulation results and experiments we showed how by simply choosing the parameters of the motion pattern it is possible to achieve a desired forward velocity for underwater snake robots. The global x axis is aligned with the desired path, and thus the position of the robot along the global y axis corresponds to the cross track error, and the heading of the robot (1) is the angle that the robot forms with the desired path (Fig. 5). The objectives of the control system can be formalized as

$$\lim_{t \to \infty} p_y = 0 \qquad (13)$$

$$\lim_{t \to \infty} \bar{\theta} = \bar{\theta}_{ss} \qquad (14)$$

$$\lim_{t \to \infty} \bar{v}_t > 0 \qquad (15)$$

where $\bar{\theta}_{ss}$ is a constant value which will be non-zero when the underwater snake robot is subjected to ocean currents that have a component in the transverse direction of the path. Note that, since underwater snake robots have an oscillatory gait pattern,
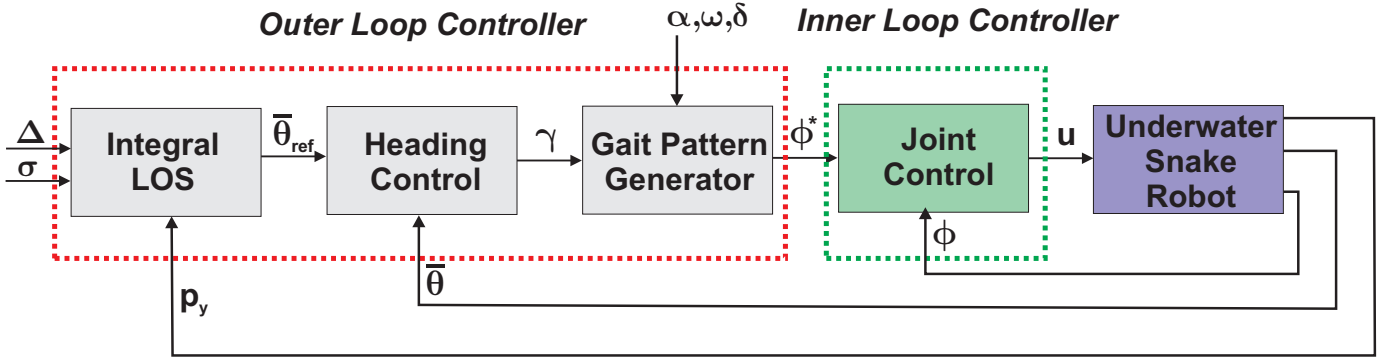
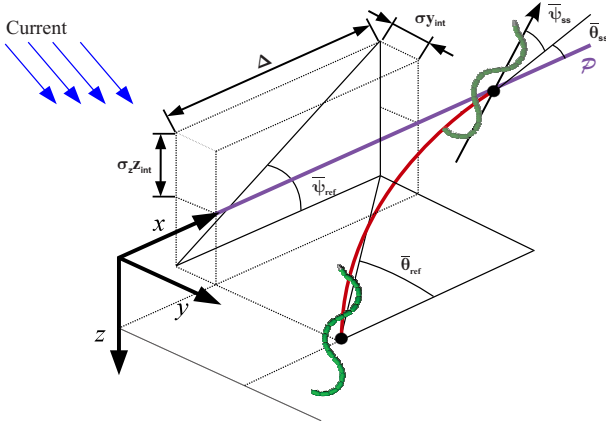Fig. 3.   The structure of the integral LOS path following controller.

Fig. 4.   Illustration of the integral LOS guidance law for motion in 3D.
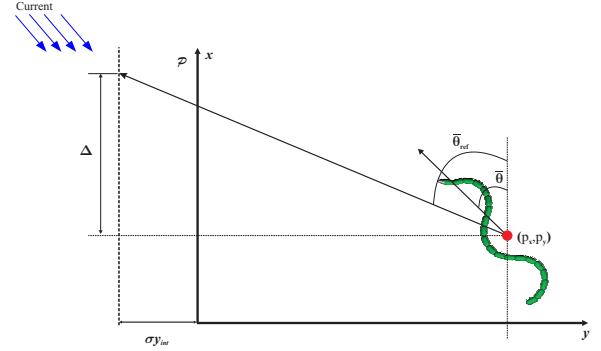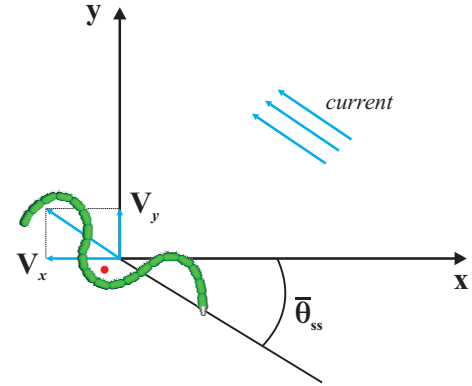

Fig. 5.   Illustration of the integral LOS guidance law for straight line path.

Fig. 6.   Steady state: The underwater snake robot side-slips with a constant $\bar{\theta}_{ss}$ to follow the path.

the control objectives imply that p_y and $\bar{\theta}$ should have steady state oscillations about zero and $\bar{\theta}_{ss}$, respectively.

Note that the heading of the robot is not required to oscillate around zero but rather to oscillate around a steady-state constant value (14) in the presence of ocean currents in the transverse direction of the path. This is similar to the results shown in [5] for autonomous surface vessels. In particular, the underwater snake robot then needs to keep a nonzero heading angle in steady state in order to compensate for the current effect. A non-zero angle will allow the underwater snake robot to side-slip in order to compensate for the current effects and thus stay on the desired path, as shown in Fig. 6.

Assumption 5. The current has unknown direction and magnitude. It should be bounded by a constant $V_{max} > 0$, i.e. $V_{max} > \sqrt{V_{x,i}^2 + V_{y,i}^2}$, where $[V_{x,i}, V_{y,i}]^T$ is the current velocity expressed in inertial frame coordinates.

Remark 4. The value of V_{max} that the robot is able to compensate is directly connected to the physical limitations of the robot, the actuator forces and the number of the links.

B. Motion Pattern

Previous studies on swimming snake robots have focused on two motion patterns; lateral undulation and eel-like motion. In this paper, we will use a general sinusoidal motion pattern that describes a broader class of motion patterns including lateral undulation and eel-like motion. Lateral undulation [9], which is the fastest and most common form of ground snake loco-motion, can be achieved by creating continuous body waves,

with a constant amplitude, that are propagated backwards from head to tail. In order to achieve lateral undulation, the snake robot is commanded to follow the serpenoid curve as proposed in [14]. Eel-like motion can be achieved by propagating lateral axial undulations with increasing amplitude from head to tail [43]. Note that simulation and experimental results for the locomotion efficiency of underwater snake robots using lateral undulation and eel-like motion patterns, both with regards to the achieved forward velocity and the average power consumption are given in [68].

In this paper, a general sinusoidal motion pattern is achieved by making each joint $i \in \{1, \cdots, n-1\}$ of the underwater snake robot track the sinusoidal reference signal

$$\phi_i^*(t) = \alpha \mathrm{g}(i,n) \sin(\omega t + (i-1)\delta) + \gamma, \qquad (16)$$

where α and ω are the maximum amplitude and the frequency, respectively, δ determines the phase shift between the joints, while the function $\mathrm{g}(i,n)$ is a scaling function for the amplitude of joint i which allows (16) to describe a quite general class of sinusoidal functions, including several different snake motion patterns. For instance, $\mathrm{g}(i,n) = 1$ gives lateral undulation, while $\mathrm{g}(i,n) = (n-i)/(n+1)$ gives eel-like motion [1]. The parameter γ is a joint offset coordinate that we will use to control the direction of the locomotion [9], [57]. In particular, in [9] and [57], γ is shown to affect the direction of locomotion in the case of land-based snake robots and fish robots, respectively.

C. Outer-Loop Controller

In previous approaches, the parameters α and δ are typically fixed and the parameters ω, γ are used to control the speed and the direction of the snake robot [9], [57], [70]. In this paper, the same idea will be used in order to steer the underwater snake robot to a desired orientation. In particular, the outer-loop controller will be responsible for generating the reference joint angles in order to ensure that the desired orientation is achieved. The orientation $\bar{\theta}$ of the robot is given by (1). Moreover, motivated by [4], [5] we propose to define the reference orientation using the following integral LOS guidance law

$$\bar{\theta}_{\mathrm{ref}} = -\arctan\left(\frac{p_y + \sigma y_{int}}{\Delta}\right), \qquad \Delta > 0 \qquad (17)$$

$$\dot{y}_{int} = \frac{\Delta p_y}{(p_y + \sigma y_{int})^2 + \Delta^2}, \qquad (18)$$

where p_y is the cross track error (i.e., the position of the underwater snake robot along the global y axis), while Δ and $\sigma > 0$ are both constant design parameters and y_{int} represents the integral action of the guidance law. In particular, Δ denotes the *look-ahead distance* that influences the rate of convergence to the desired path [67] and $\sigma > 0$ is the integral gain. The proposed integral LOS path following controller was recently proposed for path following control of marine surface vessels in presence of unknown constant irrotational ocean current [4], [5]. In particular, the integral LOS path following controller compensates for two environmental disturbances: the drifting effect of the currents, representing a pure kinematic drift, and the heading dependent disturbances caused by currents, winds and waves. This motivated us to believe that the integral LOS guidance law could be well-suited for path following of underwater snake robots in different sea conditions. In particular, the conjecture is that this choice of orientation reference will make the snake robot converge to the path, i.e. make p_y converge to zero, cf. Fig. 5. Note that, in this paper, we investigate the efficacy of the integral LOS guidance law in the presence of ocean current effects since this is the predominant environmental disturbance underwater. The applicability of the proposed control strategy for underwater snake robots under the influence of waves and other disturbances when operating in the wave zone remains a topic of future work.

Generally, the value of the parameter Δ will influence the transient motion of the robot, cf. Fig. 5. This means that it is expected to have well-damped transient motion for large values of Δ and large overshoots or even instability for too small values. Generally, for marine vehicles it is common to choose Δ larger than twice the length of the robot (see e.g.

[67]). Note that, even though the body structure and motion pattern of the robotic system studied in this paper is quite different compared to these marine vehicles, we follow the same concept for the proposed control approach. Simulations and experimental results presented in the following sections for the proposed control approach show good transient behavior of the robot by choosing $\Delta = 2ln$. In the future, optimization techniques or analytical studies can be used to investigate the influence of the parameter Δ for underwater snake robot locomotion.

Furthermore, the integral effect becomes significant when the ocean current effect pushes the underwater snake robot away from its path. Note that (18) is designed such that the integral action has less influence when the robot is far from the path, reducing the risk of wind-up effects [5]. In fact, (17, 18) behaves as a traditional LOS law when the underwater snake robot is far away from the path while the integral action takes over when the motion is closer to the desired path.

Motivated by results for ground snake robots, we seek to use the parameter γ to control the direction of the locomotion of the robot. In particular, to steer the heading $\bar{\theta}$ according to the integral LOS angle in (17), we choose the joint angle offset according to

$$\gamma = k_\theta\left(\bar{\theta} - \bar{\theta}_{\mathrm{ref}}\right), \qquad (19)$$

where $k_\theta > 0$ is a control gain [2].

D. Inner-Loop Controller

For motion in 2D, in order to make the joint angle ϕ_i follow its reference signal ϕ_i^*, a PD controller is used:

$$u_i = k_p(\phi_i^* - \phi_i) + k_d(\dot{\phi}_i^* - \dot{\phi}_i), \quad i = 1, \ldots, n-1, \quad (20)$$

where $k_p > 0$ and $k_d > 0$ are the gains of the controller.

Note that the gait parameters α, ω and δ of the general sinusoidal motion pattern (16), the controller gains k_p, k_d, k_θ in (20) and (19) and the parameters Δ and σ are chosen arbitrarily for the simulation and experimental results presented in the following sections. In the future, optimization techniques and model-based analysis approaches will be examined for choosing the gait parameters and the controller gains, respectively.

V. STABILITY ANALYSIS OF THE INTEGRAL LOS PATH FOLLOWING CONTROLLER BASED ON THE POINCARÉ MAP

In this section, the theory of Poincaré maps is employed to prove that the integral LOS path following controller proposed in Section IV generates a locally exponentially stable periodic orbit in the state space of the underwater snake robot. This periodic orbit implies that the robot locomotes along the desired straight path in the presence of current.

A. The Poincaré Map

The Poincaré map is a useful tool for studying the stability of periodic solutions in nonlinear dynamical systems [71]. In particular, the stability of a periodic orbit of a dynamical system is related to the stability of the fixed point of the corresponding Poincaré map of the system. We will thus use a Poincaré map approach as a stability analysis tool for the closed-loop system of the underwater snake robot with the path following controller presented in Section IV. In particular,

the exponential stability of the system will be investigated by checking if the fixed point is an exponentially stable equilibrium point of the discrete system. The fixed point $\bar{\mathbf{x}}^*$ is locally exponentially stable if the magnitudes of all the eigenvalues of the Jacobian linearization of the Poincaré map $\mathbf{J}_P(\bar{\mathbf{x}}^*)$ about the fixed point are strictly less than one.

Note that in order to investigate the stability properties using Poincaré maps, the model of the underwater snake robot should be represented as an autonomous system. Following the approach described in [72], the model (12) with the path following controller proposed in Section IV can be rewritten as the following autonomous system

$$\dot{\mathbf{x}} = \mathbf{F}\left(\mathbf{x}, \frac{T}{2\pi}\beta\right), \qquad \mathbf{x}(t_0) = \mathbf{x}_0$$
$$\dot{\beta} = \frac{2\pi}{T}, \qquad \beta(t_0) = \frac{2\pi t_0}{T} \tag{21}$$

where $\beta = 2\pi t/T$ is a new state variable and $T = 2\pi/\omega$ is the period of the cyclic locomotion generated by the sinusoidal gait pattern in (16). The state variable β is periodic since we force β to be $0 \leq \beta < 2\pi$, i.e. we set β to zero each time $\beta = 2\pi$.

What now remains is to specify the Poincaré section for the underwater snake robot. We choose the global x axis as the Poincaré section S of the system in (21) (see e.g. [9]). Furthermore, we exclude p_x from the Poincaré map since the forward position of the robot will not undergo limit cycle behaviour like the other states of the system. As a result, the Poincaré section is given by $S = \{(\boldsymbol{\theta}, p_y, \dot{\boldsymbol{\theta}}, \beta) | p_y = 0\}$, which means that the vector of the independent time-periodic states constrained to S can be expressed as $\bar{x} = \left[\boldsymbol{\theta}^T, \dot{\boldsymbol{\theta}}^T, \dot{\mathbf{p}}_{\text{CM}}^T, \beta\right]^T \in \mathbb{R}^{2n+3}$.

Remark 5. Note that since p_x is not present on the right hand side in any of the dynamic equations in (12), we can exclude p_x from the Poincaré map without affecting the other state variables of the system (12).

Remark 6. In this paper, we consider a one-sided Poincaré map by assuming that the Poincaré section is crossed when the CM position of the underwater snake robot crosses the x axis from above, similar to the approach presented in [9], [10] for ground snake robots.

B. Stability Analysis of the Poincaré map

In order to investigate the stability of the robot with the integral LOS path following controller proposed in Section IV, we consider an underwater snake robot with $n = 3$ links, each one having length $2l = 0.18$ m and mass $m = 0.8$ kg. The hydrodynamic parameters are $c_t = 0.4453$, $c_n = 15.84$, $\mu_n = 1.7106$, $\lambda_1 = 5.2604\text{E}{-}8$, $\lambda_2 = 0.0012$ and $\lambda_3 = 8.1160\text{E}{-}5$. The drag fluid parameters c_t and c_n are calculated for $C_d = 1.6$ and $C_f = 0.03$. An extensive discussion about the values of the fluid parameters can be found in [1]. The values of a constant ocean current in the inertial frame are $[0.005, 0.01]$ m/sec. The joint PD controller (20) is used for each joint with parameters $k_p = 20$, $k_d = 5$, and lateral undulation and eel-like motion are achieved by choosing $\text{g}(i,n) = 1$ and $\text{g}(i,n) = (n-i)/(n+1)$, respectively, with gait parameters $\alpha = 70^\circ$, $\delta = 70^\circ$ and $\omega = 120^\circ/\text{s}$ in (16). Initially, we run simulations with the proposed control strategy until the robot reaches the desired path, and then we choose the initial values of y_{int} as 4.97 and 4.84 for lateral undulation and eel-like motion, respectively. Note that these initial values are
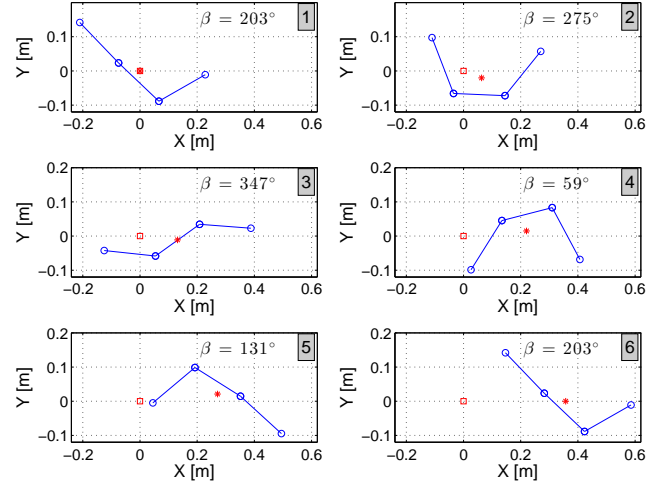

Fig. 7. Motion of the underwater snake over one period of the cyclic locomotion T, with the new state variable $\beta = 2\pi t/T$ for lateral undulation. The red rectangle and star represent the initial position and the position of the CM at the time of the screenshot, respectively.

used for the stability analysis of the system by using Poincaré map. Furthermore, the control gain in (19) is $k_\theta = 0.8$, while the guidance law parameters in (17-18) are chosen as $\Delta = 2ln$ [67], and $\sigma = 0.01$ [5].

The Poincaré map of the underwater snake robot model in (10, 11) is found using Matlab R2013b. The dynamics is calculated using the ode23tb solver with a relative and absolute error tolerance of $1\text{E}{-}4$. Using the Newton-Raphson algorithm, the fixed point, $\bar{\mathbf{x}}^* \in \mathbb{R}^9$, of the Poincaré map for lateral undulation and eel-like motion are given by (22) and (23), respectively:

$$\bar{\mathbf{x}}^* = [-41.01^\circ, -38.56^\circ, 25.54^\circ, -102.75^\circ/\text{s}, 35.44^\circ/\text{s},$$
$$99.38^\circ/\text{s}, 14.76\text{cm/s}, -5.62\text{cm/s}, 202.55^\circ]^T \tag{22}$$

$$\bar{\mathbf{x}}^* = [-50.64^\circ, -17.01^\circ, 20.63^\circ, -76.21^\circ/\text{s},$$
$$47.03^\circ/\text{s}, 46.81^\circ/\text{s}, 12.04\text{cm/s}, -3.51\text{cm/s}, 233.30^\circ]^T \tag{23}$$

The locomotion of the robot over one period is shown in Fig. 7 and Fig. 8 for lateral undulation and eel-like motion, respectively. The initial values of the states of the robot are given by (22) and (23), and the initial position is chosen as $\mathbf{p}_{\text{CM}} = 0$. From Fig. 7-8, we can see that after one period of the motion the state variables have returned to their initial values given by (22) and (23). In addition, after one period of motion the position of the robot along the x axis has increased. Furthermore, Fig. 9a and Fig. 10a illustrate the limit cycle that is traced out by the three link angles of the robot for lateral undulation and eel-like motion.

The Jacobian linearization of the Poincaré map about the fixed points (22) and (23) is calculated, and the magnitudes of the eigenvalues of $\mathbf{J}_P(\bar{\mathbf{x}}^*) \in \mathbb{R}^{9 \times 9}$ are found to be given by (24) and (25) for lateral undulation and eel-like motion, respectively:

$$| \text{eig}(\mathbf{J}_P(\bar{\mathbf{x}}^*)) | = [0.364, 0.196, 0.196, 0.030, 0.003,$$
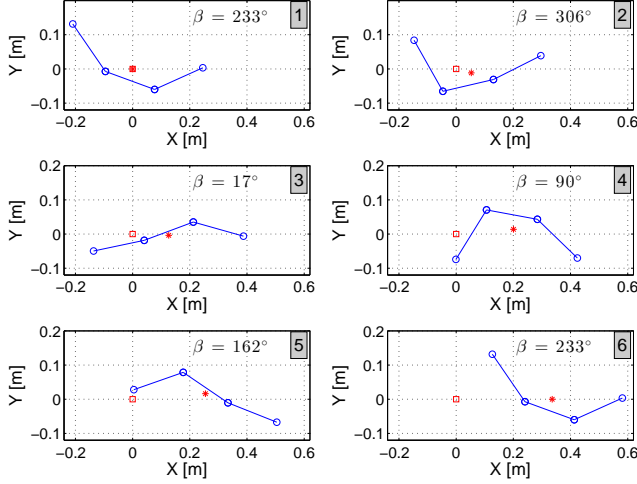$$0.0014, 1.59\text{E}{-}6, 1.53\text{E}{-}4, 3.84\text{E}{-}4]^T \tag{24}$$

Fig. 8. Motion of the underwater snake over one period of the cyclic locomotion T, with the new state variable $\beta = 2\pi t/T$ for eel-like motion. The red rectangle and star represent the initial position and the position of the CM at the time of the screenshot, respectively.

$$| \text{eig}(\mathbf{J}_P(\bar{\mathbf{x}}^*)) |= [0.875, 0.875, 0.041, 0.0059, 0.0059,$$
$$8.62\text{E}-4, 1.57\text{E}-4, 1.88\text{E}-5, 2.71\text{E}-4]^T \tag{25}$$

From (24) and (25), it is easily seen that all the eigenvalues, both for lateral undulation and eel-like motion cases, are strictly less than one. Therefore we can conclude that the periodic orbit is locally exponentially stable for the given choice of controller parameters both for lateral undulation and eel-like motion. Since the periodic orbit is exponentially stable and the system returns to $p_y = 0$ with time period T, we can conclude that the control objective (13) is achieved. Furthermore, in [73] it is shown that, for an underwater snake robot under anisotropic drag effects, propulsive forces are positive as long as $\text{sgn}(\theta_i) = \text{sgn}(\dot{y}_i)$ and $\text{sgn}(\theta_i) = \text{sgn}(\ddot{y}_i)$. Fig. 9b-9c and Fig. 10b-10c show that these conditions are valid over the majority of the period for both lateral undulation and eel-like motion. Hence, the robot moves forward and the control objective (15) is satisfied. Since the control objectives (13) and (15) are both satisfied, we can argue that the control objective (14) must be satisfied. Note that if the heading did not oscillate around $\bar{\theta}_{ss}$, but rather around zero, then the robot would not be able to compensate the ocean current effects and the robot would drift away from the desired path, which contradicts the fulfilment of control objective (13).

Remark 7. A more formal stability analysis of the system in (10, 11) with the proposed controller remains a challenging task, mainly due to the complexity of the dynamic system equations [1]. Thus a numerical approach is adopted in this paper. Note that by using the Poincaré map approach, we have only proven that the stability of the proposed path following controller presented in Section IV holds for the numerical parameters of the system presented in the beginning of this subsection. However, simulations indicate that the proposed path following controller can be applied to steer the robot to the desired path in the presence of ocean currents for other parameters of the system and for a wide range of the current values.

VI. SIMULATION STUDY

This section presents simulation results in order to investigate the performance of the integral LOS path following controller described in Section IV. The model and controller parameters are the same as in Section IV. The initial values of all states of the robot are set to zero except for the initial position of the center of mass, which is selected as $p_{CM}(0) = [0, 0.5]$. In Fig. 11a and Fig. 12a, we can see that (19) makes the heading angle converge to and oscillate about the desired heading angle given by (17) for lateral undulation and eel-like motion, respectively. Note that the heading of the robot does not converge to oscillations about zero but rather converges to a steady state constant value, $\bar{\theta}_{ss}$, which means that the control objective (14) is achieved. Moreover, Fig. 11b and Fig. 12b show that control objective (13) is verified, i.e. the integral LOS guidance law (17) will make the cross track error converge to zero. Finally, from Fig. 11c and Fig. 12c we can see that the CM of the underwater snake robot converges to the desired path for both lateral undulation and eel-like motion. Fig. 11-12 clearly show that the heading, the cross track error and the position of the robot have a steady state oscillatory behavior when the robot reaches the desired path, as described in Section IV.A.

VII. EXPERIMENTAL INVESTIGATION

This section describes the experimental setup employed in order to investigate the performance of the integral LOS path following controller proposed in [2], and the experimental results.

A. Underwater Snake Robot – Mamba

In this section, the underwater snake robot that was used in our experiments is presented. A more detailed description of the robot is found in [6].

The snake robot Mamba (Fig. 13) is a mechanically robust and easily reconfigurable experimental platform developed to support our ongoing research on ground and underwater snake robot locomotion. The robot is watertight and has a modular design with a common mechanical and electrical interface between the modules. Each joint module is actuated by a Hitec servo motor (HSR 5990TG). The sensors inside each joint include a force/torque sensor on the joint shaft, two temperature sensors, a 3-axis accelerometer, and a water leakage detector. The joint is controlled using a microcontroller card (TITechSH2 Tiny Controller from HiBot), which communicates with other modules over a CAN bus. Power supply cables (35 V) run between the modules along with the CAN bus.

Note that even though all the modules of the robot are watertight down to about 5 m, the robot was covered by a watertight skin during the underwater path following experiments to achieve an extra water barrier (Fig. 13). Moreover, the skin gives the robot a smoother outer surface, thereby reducing the drag effects. The skin is made of Groundsheet, Nylon, PU-coated, 90 g/m^2 material and it is attached at the head and the tail parts using silicone rubber seals made from Dragon Skin Series product [74].
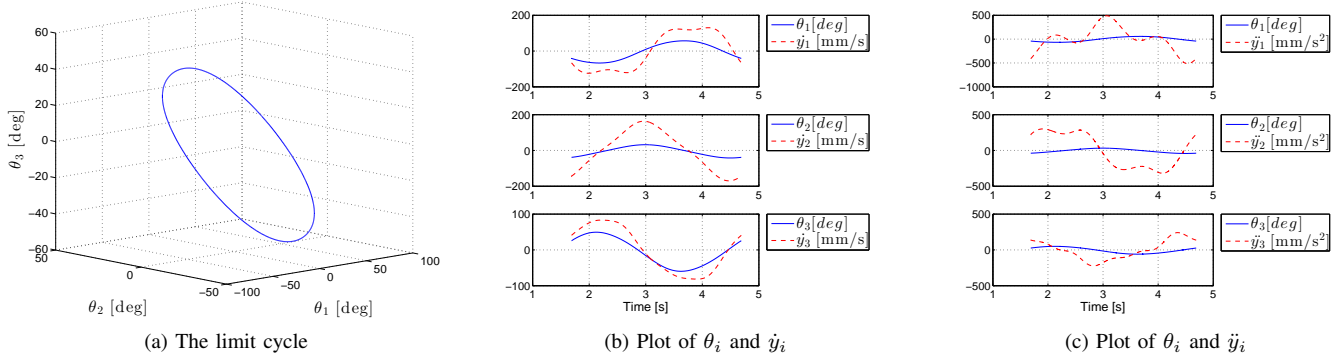
(a) The limit cycle

(b) Plot of θ_i and $\dot{y}_i$

(c) Plot of θ_i and $\ddot{y}_i$

Fig. 9. Stability analysis of the Poincaré map for lateral undulation.

(a) The limit cycle

(b) Plot of θ_i and $\dot{y}_i$

(c) Plot of θ_i and $\ddot{y}_i$
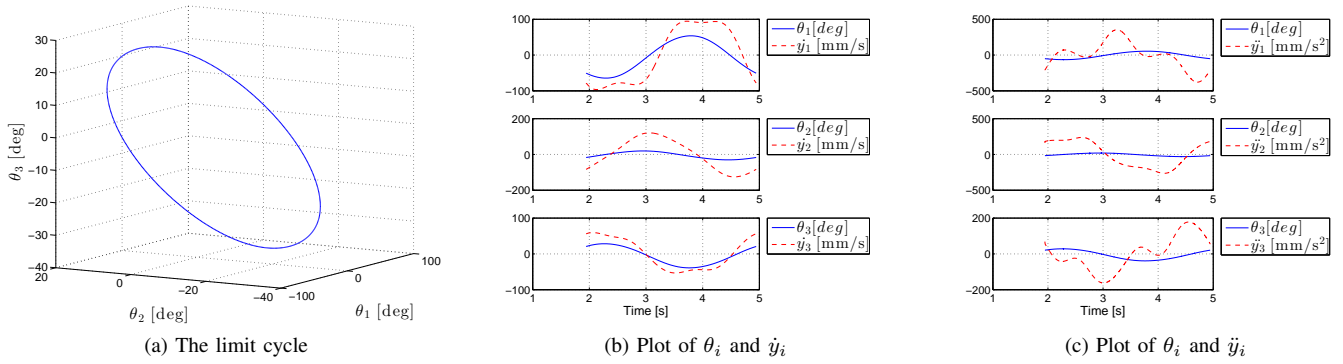
Fig. 10. Stability analysis of the Poincaré map for eel-like motion.

(a) Heading angle, $\bar{\theta}$

(b) Cross track error, p_y

(c) The path of the robot, where the configuration of the robot at different time steps is represented in blue
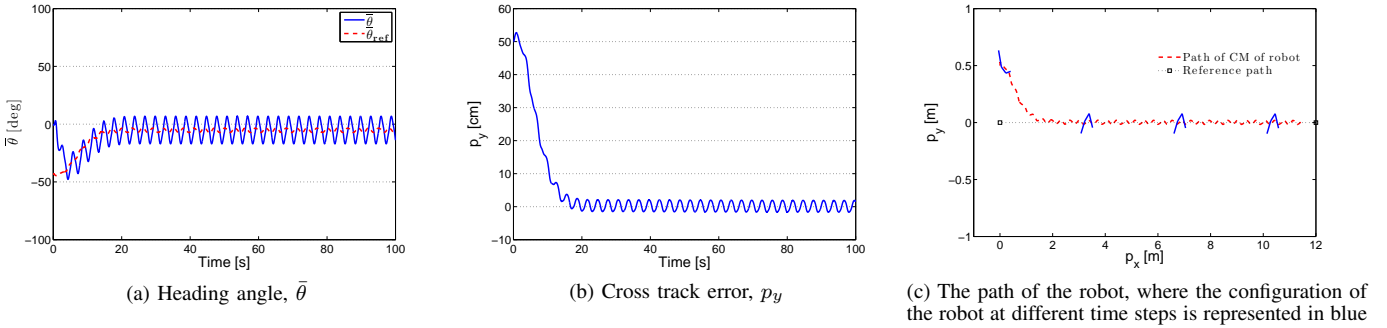
Fig. 11. Integral LOS path following controller for lateral undulation.

(a) Heading angle, $\bar{\theta}$

(b) Cross track error, p_y

(c) The path of the robot, where the configuration of the robot at different time steps is represented in blue
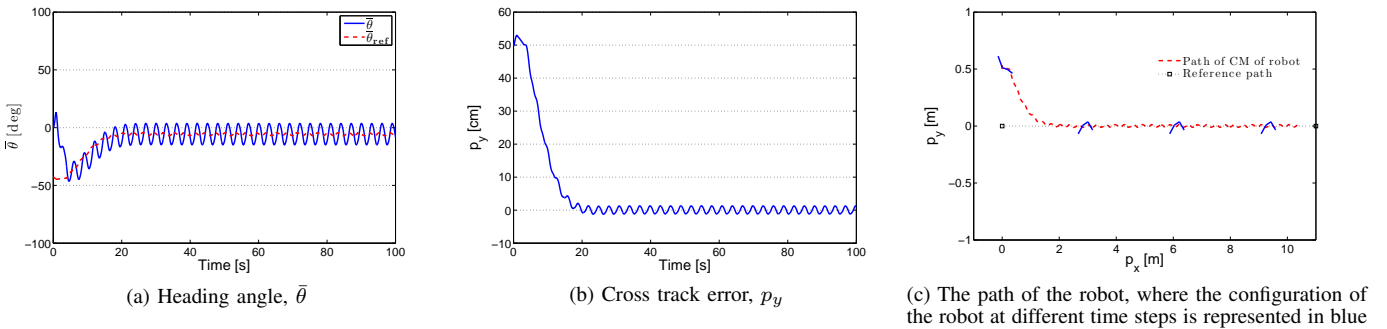
Fig. 12. Integral LOS path following controller for eel-like motion.
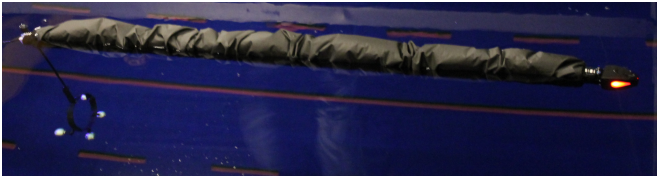
Fig. 13. The underwater snake robot Mamba in the pool with the markers attached on the tail for position measurements.

B. Experimental Setup

The performance of the guidance strategy presented in Section IV was investigated experimentally for straight line paths. The experiments were performed in the North Sea Center Flume Tank in Hirtshals, Denmark [75]. The dimensions of the tank are L: 30 m, H: 6 m and W: 8 m and an installation of four propellers and motors of 64 kW in the tank provides the ability to generate water flow up to 1 m/sec. In addition, the tank is equipped with a state-of-the-art motion capture system from Qualisys [76], which provides accurate real time measurements of the position and orientation of underwater objects equipped with reflective markers.

The experiments were carried out using the underwater snake robot – Mamba (Fig. 13) [6], with 18 identical joint modules mounted horizontally and vertically in an alternating fashion. During the experiments, the robot was moved according to a strictly horizontal motion pattern where the joints with vertical axis were constrained at zero degrees. The kinematics of the snake robot therefore corresponded to a planar snake robot with links of length $2l_i = 0.18$ m and mass $m_i \approx 0.8$ kg. During the experiments, the robot had a slightly positive buoyancy and was swimming near the water surface. In order to measure the position and the orientation of the snake robot, reflective markers were attached on the tail part of the robot, as shown in Fig. 13. Although the robot was swimming on the surface of the tank, the markers were submerged in the tank approximately 0.5 m from the surface since the camera system was unable to track markers above 0.5 m from the surface. The global frame coordinates of the tail link and the absolute angle of the tail were measured using the camera-based motion capture system from Qualisys [76] installed in the tank. The camera system consisted of six cameras, which allow reflective markers to be tracked under water. The controller structure used in the experiments is illustrated in Fig. 14. The measured position and the absolute angle of the tail were received from an external computer where the Qualisys system [76] was connected, and afterwards these measurements were sent through UDP in LabVIEW 2013 to another computer where the path following controller was implemented.

Knowing the position and the orientation of the tail of the robot, and also the individual joint angles, and by using the kinematics of the robot presented in Section III, the center of mass position, $\mathbf{p}_{\mathrm{CM}}$ and the absolute link angles, $\boldsymbol{\theta}$ of the underwater snake robot were calculated. The integral LOS path following controller of the underwater snake robot was implemented on an external computer according to (16), (17), (18) and (19) for the lateral undulation gait pattern. The solutions of (18) were obtained by numerical integration in LabVIEW 2013, which was used as the development environment for the path following controller. The reference joint angles, computed by (16), were sent to the robot via a CAN bus and the joint

angles were controlled according to a proportional controller implemented in the microcontroller of each joint module. The reference angles are sent to the robot from an external PC at the frequency 10 Hz. Note that we did not implement the joint torque controller given by (20) since accurate torque control is not supported by the servo motors installed in the snake robot. The orientation of the robot was estimated according to (1), i.e. as the average of the individual link angles. The integral LOS angle given by (17) was calculated with a look-ahead distance equal to the length of the robot, i.e. $\Delta = 1.6$ m [67] for fast convergence due to the limited length of the tank, and $\sigma = 0.01$ [5]. Furthermore, the initial values of y_{int} were zero and the control gain in (19) was $k_\theta = 0.3$. The joint angle offset was saturated according to $\phi_0 = [-20^o, 20^o]$ in order to keep the joint reference angles within reasonable bounds with respect to the maximum allowable joint angles of the physical robot.

The reference angles corresponding to the horizontal joint motion of the robot were calculated according to (16) with $n = 9$ by choosing $\mathrm{g}(i, n) = 1$ and gait parameters $\alpha = 30^o$ and $\delta = 40^o$, while $\omega = 80^o/s$ and $\omega = 90^o/s$ are chosen for the LOS and integral LOS path following controller, respectively. The reference angles corresponding to the vertical joint motion were zero in order to constrain the motion of the robot purely in the horizontal plane. Furthermore, the initial values of the link angles were set to zero, while the initial heading and position of the robot are presented in each trial. Note that the forward speed of the robot in the experiments was set at a moderate level to prevent the motors in the joints from overheating.

As previously mentioned, in order to measure the position and the orientation of the robot, reflective markers were attached on the tail module of the robot using an external structure. In order to avoid any misplacement of the markers and thus get accurate measurements from the underwater camera system, we implemented a lightweight and stiff structure made from iron ropes in which the markers were attached. Note that the markers were attached on the tail module and not at the CM of the robot mainly to reduce any extra disturbances produced from the motion of the robot that would influence all the links from the middle joint and backwards due to the external structure. However, the implemented structure has reasonable dimensions in order to reduce the effect on the motion of the robot.

C. Experimental Results

The straight line path following controller was experimentally investigated for the following two different cases.

1) LOS path following controller: Initially, we performed experiments with no current effects and $\sigma = 0$. In this case, the guidance strategy is reduced to the well-known LOS path following guidance law [67]. Experimental results for three different sets of initial conditions are presented. In the first two trials of the experiments, the robot was initially headed along the desired path (the x axis), and the initial distance from the CM to the desired path was 0.2555 m and 0.4926 m, respectively. In the last trial, the robot was initially headed towards the desired path (the x axis) with initial heading $\bar{\theta}(0) = -91.2^o$, and the initial distance from the CM to the desired path was -0.3698 m.

The experimental results for the three trials are presented in Fig. 15-17, where it is easily seen that the robot converged
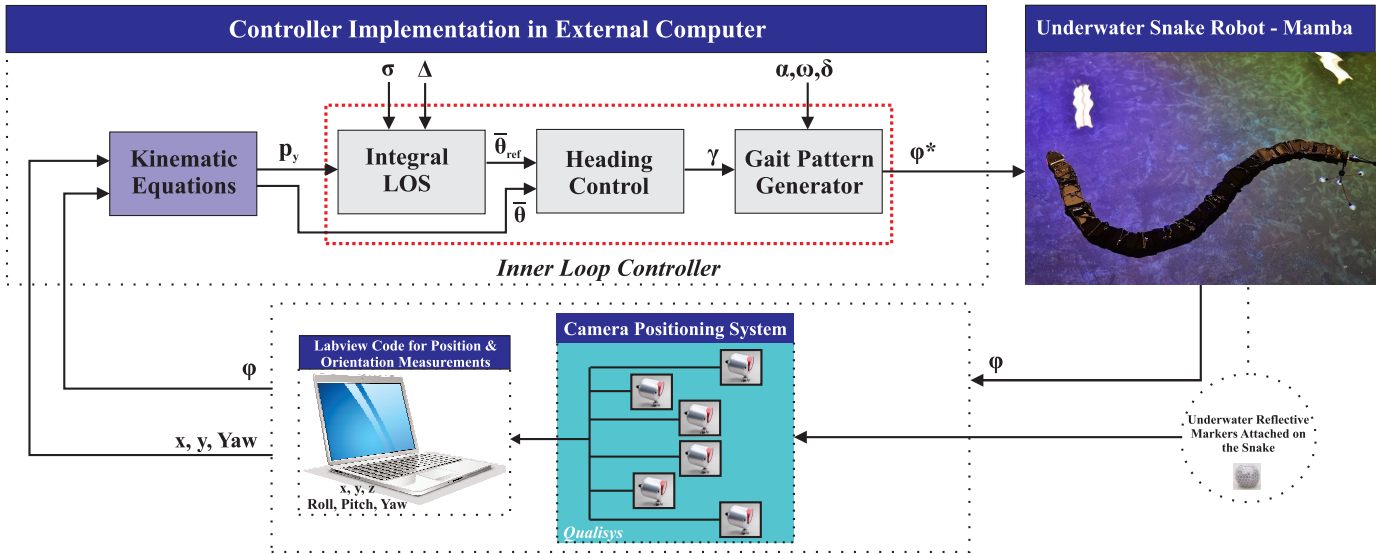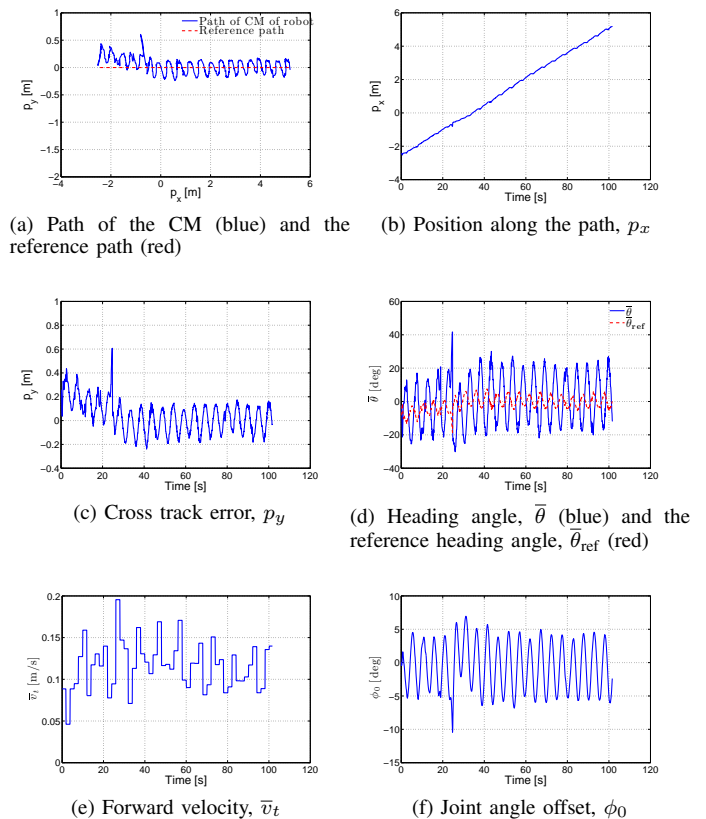
Fig. 14. Illustration of the controller structure used in the experiments.

nicely towards and moved along the desired path during all three trials. In Fig. 15d, Fig. 16d and Fig. 17d we can see that (19) makes the heading angle converge to and oscillate about zero for lateral undulation. Note that the measured orientation oscillated with a larger amplitude than the reference orientation. The reason for this deviation is that there is no clear general definition of the heading of the snake robot. In particular, the snake robot consists of multiple individual links, where each link has its own individual heading. In this paper, we have chosen a measure of orientation for the whole robot based on the average of the link angles. While this measure in average corresponds to the direction in which the CM is displaced (which is what the reference heading is commanding), it will still oscillate due to the oscillating motion of the links. For this reason, our claim is that the heading of the snake robot is successfully tracking the reference heading as long as the heading is oscillating about the reference. Moreover, Fig. 15c, Fig. 16c and Fig. 17c show that the cross track error converges to and oscillates about zero. Finally, from Fig. 15a, Fig. 16a and Fig. 17a we can see that the center of mass of the underwater snake robot converges to the desired path for lateral undulation. Furthermore, the forward velocity of the robot is shown in Fig. 15e, Fig. 16e and Fig. 17e and the joint angle offset is shown in Fig. 15f, Fig. 16f and Fig. 17f.

Fig. 15-17 clearly show that the heading, the cross track error and the position of the robot have a steady state oscillatory behavior when the robot reaches the desired path. Note that this was expected since for an underwater snake robot with revolute joints, it is difficult to achieve a purely non-oscillating motion of the CM. Similar to the oscillatory behaviour of the CM, the orientation of the robot was also expected to oscillate, as it is shown in Fig. 15d, Fig. 16d and Fig. 17d.

2) Integral LOS path following controller: We investigated the performance of the proposed control strategy for a constant current in the inertial frame. Using the flow water speed generator this was set equal to $[-0.07\cos(45^o), -0.07\sin(45^o)]$ m/sec. This was achieved by defining the straight line path at a 45 degree angle with respect to the direction of the water flow and setting the water flow speed to 0.07 m/sec. The straight

(a) Path of the CM (blue) and the reference path (red)

(b) Position along the path, p_x

(c) Cross track error, p_y

(d) Heading angle, $\overline{\theta}$ (blue) and the reference heading angle, $\overline{\theta}_{\text{ref}}$ (red)

(e) Forward velocity, $\overline{v}_t$

(f) Joint angle offset, ϕ_0

Fig. 15. LOS straight line path following with the physical snake initially headed along the desired path with the initial distance from the CM being $p_y = 0.2555$ m.

line path following controller was experimentally investigated from two different sets of initial conditions. In both trials, the robot was headed along the desired path (the x axis), and the initial distance from the CM to the desired path was -1.5728 m and -0.7661 m, respectively. In Fig. 18d and Fig. 19d we can see that (19) makes the heading angle converge
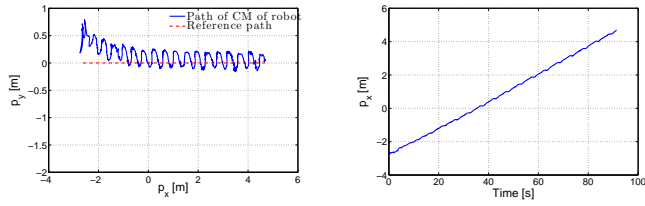
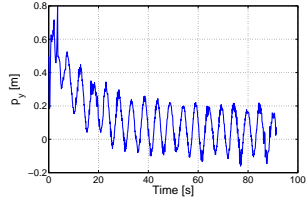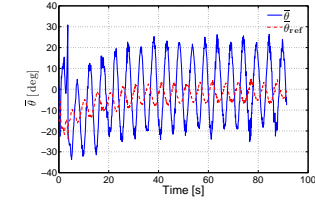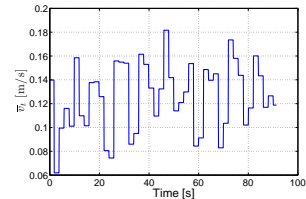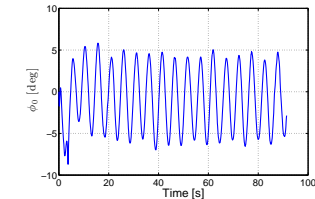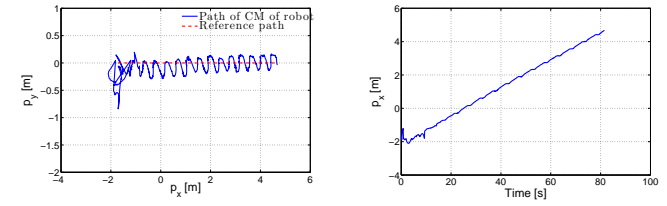(a) Path of the CM (blue) and the reference path (red)

(b) Position along the path, p_x

(c) Cross track error, p_y

(d) Heading angle, $\overline{\theta}$ (blue) and the reference heading angle, $\overline{\theta}_{\text{ref}}$ (red)

(e) Forward velocity, $\overline{v}_t$

(f) Joint angle offset, ϕ_0

Fig. 16. LOS straight line path following with the physical snake initially headed along the desired path with the initial distance from the CM being $p_y = 0.4926$ m.

(a) Path of the CM (blue) and the reference path (red)

(b) Position along the path, p_x

(c) Cross track error, p_y

(d) Heading angle, $\overline{\theta}$ (blue) and the reference heading angle, $\overline{\theta}_{\text{ref}}$ (red)

(e) Forward velocity, $\overline{v}_t$

(f) Joint angle offset, ϕ_0

Fig. 17. LOS straight line path following with the physical snake initially headed towards the desired path with the initial heading and the initial distance from the CM being $\overline{\theta}(0) = -91.2^o$ and $p_y = -0.3698$ m, respectively.

to and oscillate about the desired heading angle given by (17) for lateral undulation. Note that the desired heading of the robot does not converge to oscillations about zero, but rather converges to a steady state constant value $\overline{\theta}_{ss}$ to compensate for the effect of the water current. Moreover, Fig. 18c and Fig. 19c show that the cross track error converges to and oscillates about zero. Finally, from Fig. 18a and Fig. 19a, we can see that the center of mass of the underwater snake robot converges to the desired path for lateral undulation. We see in Fig. 18a and Fig. 19a that there is a small overshoot as the snake robot converges to the path. This is a result of the tuning, and in particular the choice of the look-ahead distance Δ. The larger the choice of Δ is, the smaller the overshoot will be, and the slower the convergence rate will be. The choice of Δ is thus a trade-off between convergence rate on the one hand and the overshoot on the other hand. Furthermore, the forward velocity of the robot is shown in Fig. 18e and 19e and the joint angle offset is shown in Fig. 18f and 19f.

The visualisation in Fig. 20 for the results presented in Fig. 19 illustrates that the robot converged nicely towards and moved along the desired path. This claim is supported by the plots of the cross track error in Fig. 19c, which shows that the cross track error converges to and oscillates about zero. Fig. 18-19 clearly show that the heading, the cross track error and the position of the robot have a steady state oscillatory behavior when the robot reaches the desired path, similar to the results presented for the LOS path following controller.

3) Simulation Results: In order to perform a back-to-back comparison of real experimental and ideal simulation results,
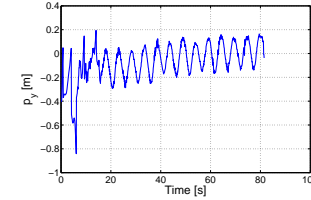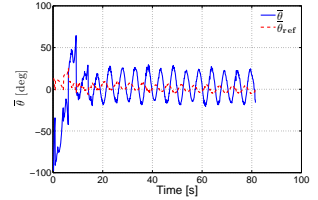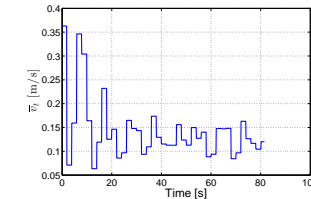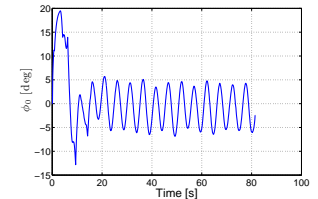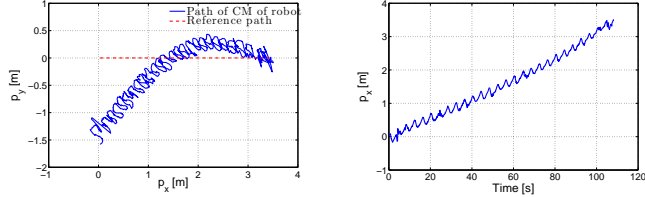
we simulate the model presented in Section III with the integral LOS path following controller proposed in Section IV using similar parameters. In particular, we consider an underwater snake robot with $n = 9$ links, each one having length $2l = 0.18$ m and mass $m = 0.8$ kg, i.e. identical to the physical robot presented in Section VI.A. The hydrodynamic parameters are set to values presented in Section V.B. The values of a constant ocean current in the inertial frame are $[-0.17, -0.17]$ m/sec. The joint PD controller (20) is used for each joint with parameters $k_p = 20$, $k_d = 5$, and lateral undulation is achieved by choosing $g(i, n) = 1$, with gait parameters $\alpha = 30^o$, $\delta = 40^o$ and $\omega = 90^o/s$ in (16). Furthermore, the control gain in (19) is $k_\theta = 0.3$, while the guidance law parameters in (17-18) are chosen as $\Delta = 1.6$ [67], and $\sigma = 0.08$ [5]. The initial values of all states of the robot are set to zero except for the initial position of the center of mass, which is selected as $p_{CM}(0) = [-1.2375, -0.7661]$, i.e. same as the initial values presented for the case shown in Fig. 19. The simulation results are shown in Fig. 21.

Following the same approach presented in Section V, the fixed point of the Poincaré map for lateral undulation for a robot with 9 links is given by

$$
\begin{aligned}
\overline{\mathbf{x}}^* = [&-14.19^o, -9.75^o, 12.03^o, 41.90^o, 66.83^o, 76.06^o, \\
&66.13^o, 42.58^o, 17.32^o, -23.23^o/s, 21.66^o/s, 54.55^o/s, \\
&60.89^o/s, 38.41^o/s, -1.56^o/s, -39.26^o/s, -56.02^o/s, \\
&-43.13^o/s, 3.88\text{cm/s}, -3.49\text{cm/s}, 207.60^o]^T.
\end{aligned}
$$

$$(26)$$

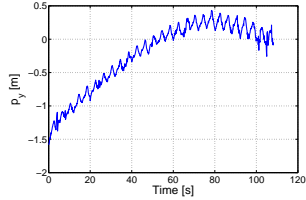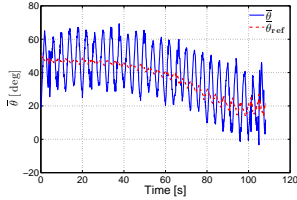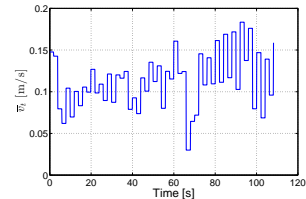(a) Path of the CM (blue) and the reference path (red)

(b) Position along the path, p_x

(c) Cross track error, p_y

(d) Heading angle, $\overline{\theta}$ (blue) and the reference heading angle, $\overline{\theta}_{\text{ref}}$ (red)

(e) Forward velocity, $\overline{v}_t$

(f) Joint angle offset, ϕ_0

Fig. 18. Integral LOS straight line path following with the physical snake initially headed along the desired path with the initial distance from the CM being $p_y = 1.5728$ m.
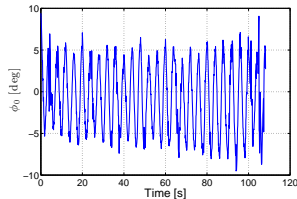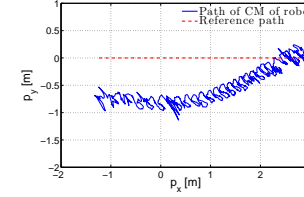
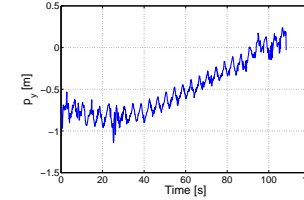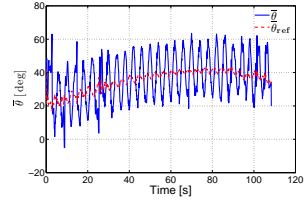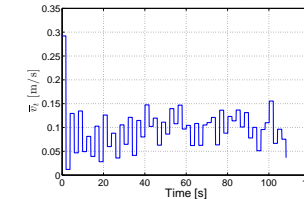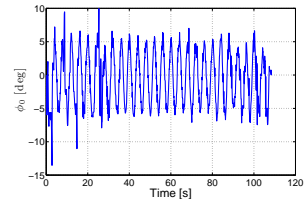(a) Path of the CM (blue) and the reference path (red)

(b) Position along the path, p_x

(c) Cross track error, p_y

(d) Heading angle, $\overline{\theta}$ (blue) and the reference heading angle, $\overline{\theta}_{\text{ref}}$ (red)

(e) Forward velocity, $\overline{v}_t$

(f) Joint angle offset, ϕ_0

Fig. 19. Integral LOS straight line path following with the physical snake initially headed along the desired path with the initial distance from the CM being $p_y = -0.7661$ m.

Fig. 22 shows the limit cycles that are traced out by the 9 links of the robot for lateral undulation. Afterwards, the Jacobian linearization of the Poincaré map about the fixed point (26) is calculated. The magnitudes of the eigenvalues are found to be given by

$$| \operatorname{eig}(\mathbf{J}_P(\bar{\mathbf{x}}^*)) | = [0.500, 0.116, 0.0103, 0.005, 0.005,$$

$7.53\mathrm{E}{-}4,\ 2.92\mathrm{E}{-}4,\ 2.06\mathrm{E}{-}4,\ 1.14\mathrm{E}{-}4,\ 7.83\mathrm{E}{-}5,\ 1.03\mathrm{E}{-}5,$

$2.77\mathrm{E}{-}6,\ 2.77\mathrm{E}{-}6,\ 1.51\mathrm{E}{-}6,\ 1.39\mathrm{E}{-}6,\ 7.57\mathrm{E}{-}7,\ 1.85\mathrm{E}{-}7,$

$1.55\mathrm{E}{-}7,\ 1.55\mathrm{E}{-}7,\ 7.75\mathrm{E}{-}8,\ 7.75\mathrm{E}{-}8]^T.$

(27)

As we can see from (27), all the eigenvalues are strictly less than one. Hence, we can conclude that the periodic orbit is locally exponentially stable for the given choice of the controller parameters for a system identical to the physical robot studied in this paper for lateral undulation motion pattern.

D. Discussion

The results shown in Fig. 19 and Fig. 21 indicate that the qualitative behavior of the simulated system is similar to the behavior of the physical robot. In addition, tuning the values of the current for the simulated system, we also achieve a good quantitative similarity between the simulated and experimental results. In particular, from Fig. 19a and Fig. 21a it can be seen that the physical snake and the simulated snake follow almost the same path. The cross track error converges and oscillates about zero in both cases in the same time horizon,

as shown in Fig. 19c and Fig. 21c. In Fig. 19c the cross track error has larger oscillations compared to the ideal case in Fig. 21c and this was expected mainly due to the noise on the measurements in the experiments caused by different sensors i.e. the position measurement from the camera system and the joint angle measurements from the actuators. In addition, it is worth mentioning that the integral LOS was implemented in Labview via numerical integration and the integration of noisy data produces errors that can cause these oscillations. From Fig. 19d and Fig. 21d, we see that in both cases the heading converges to a constant steady state value of 38°, approximately. The oscillation of the heading is larger in Fig. 19d than in Fig. 21d and this is again due to the inaccuracies of the different measurements from the sensors. Note that the heading is defined as the average of the link angles (1) and any inaccurate measurements from the encoders will produce errors and this is the main reason for the larger oscillations on the heading in the experimental results presented in Fig. 19d.

Although an ocean current with values $[-0.07\cos(45^o), -0.07\sin(45^o)]$ m/sec was generated in the flume tank, the experiments were performed on the surface of the flume tank where also surface effects and possibly also wave drift influenced the motion of the robot. Furthermore, the attachment system that is used for the markers on the tail of the robot also affects the motion of the robot. In addition, it is expected that the robot is influenced from other hydrodynamic effects which are produced through to the interaction of the robot and the surrounding fluid one
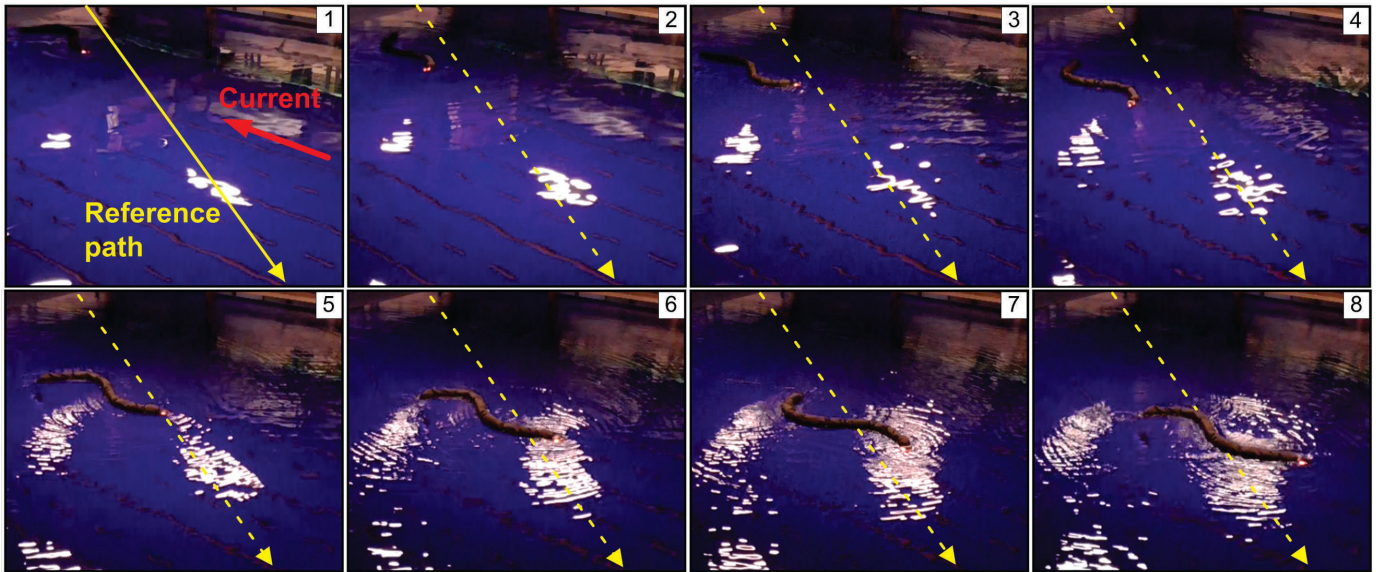
Fig. 20. The motion of the underwater snake robot during path following for the experimental results presented in Fig. 19. The *yellow line* indicates the desired path, i.e. the global x axis, and the *red line* the constant irrotational current direction.

the surface, and which are not taken into account in the proposed modeling approach for underwater snake robots presented in [1]. The actual values of the total drift effects experienced by the snake robot are therefore not precisely known. In order to find an estimate of the total drift effects, we use that $\bar{\theta}_{ss}$ is directly related to the values of the drift effects that the system is experiencing, (see [5] for more details on this). We can thus find an estimate of the drift effects by tuning the ocean current (drift) parameters until they produce the same $\bar{\theta}_{ss}$ as observed in the experiments. This gives the resulting ocean drift values $[-0.17, -0.17]$ m/sec which are then used in the simulations. As we can see from Fig. 19 and Fig. 21, for these values there is a good match between the simulation and experimental results.

However, it is worth mentioning that results presented in Fig. 18, Fig. 19 and Fig. 21 indicate that the proposed integral LOS path following controller successfully steered the underwater snake robot towards and along the desired straight path, compensating for the unknown hydrodynamic disturbances by keeping a constant non-zero heading. This makes the proposed control strategy applicable for motion planning of underwater snake robots under the influence of constant irrotational ocean currents and other ocean drift effects.

VIII. CONCLUSION

In this work experimental results for both line-of-sight and integral line-of-sight path following control of underwater snake robots were presented. In particular, a straight line path following controller was proposed for an underwater snake robot in the presence of constant irrotational currents of unknown direction and magnitude. The integral LOS guidance law was combined with a directional controller to steer the robot to the path, where the integral action in the guidance law produced a constant side-slip angle that allowed the control system to compensate for the ocean current effect. The proposed path following controller consists of three main components: a) the gait pattern controller, which produces a sinusoidal motion pattern which propels the robot forward

(a) Path of the CM (blue) and the reference path (red)

(b) Position along the path, p_x

(c) Cross track error, p_y

(d) Heading angle, $\bar{\theta}$ (blue) and the reference heading angle, $\bar{\theta}_{\text{ref}}$ (red)

(e) Forward velocity, $\bar{v}_t$

(f) Joint angle offset, ϕ_0
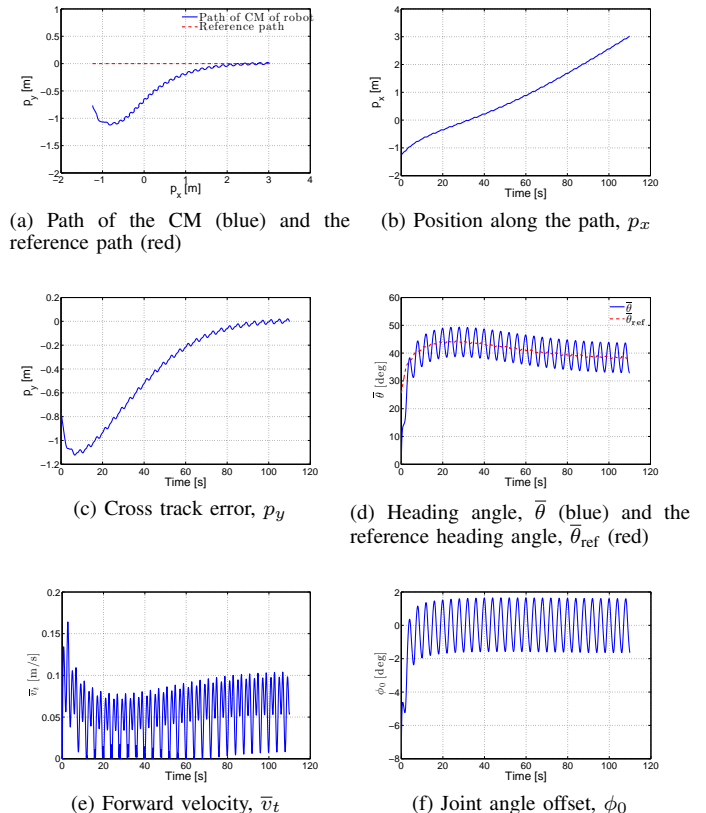
Fig. 21. Simulation results for the integral LOS straight line path following for a snake robot with $n = 9$ links initially headed along the desired path with the initial distance from the CM being $p_y = -0.7661$ m.

(16), b) the heading controller, which steers the robot towards and subsequently along the desired path (19) and c) the integral LOS guidance law, which generates the desired heading angle in order to follow the desired path (17,18). It was shown that the proposed control scheme can be applied to underwater

(a) θ_1, θ_2 and θ_3

(b) θ_4, θ_5 and θ_6

(c) θ_7, θ_8 and θ_9
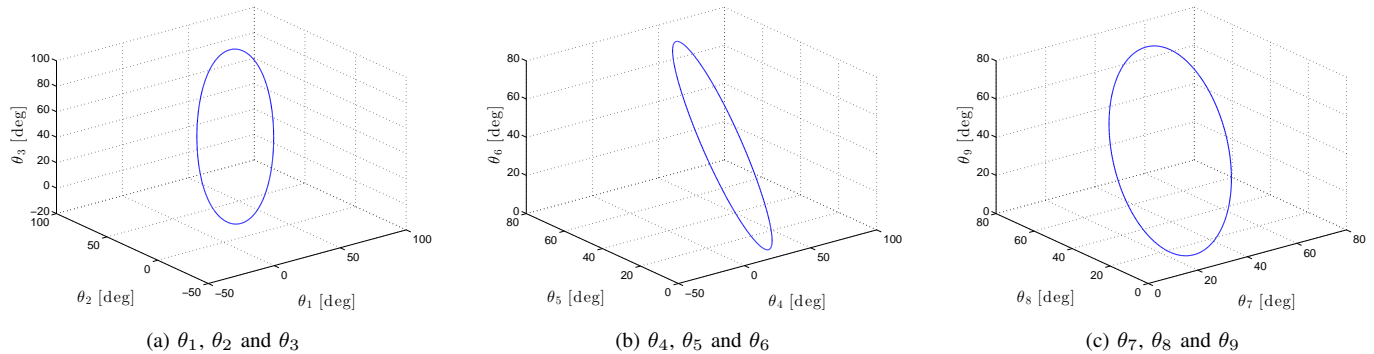
Fig. 22. The limit cycle for lateral undulation.

snake robots to compensate for the current effect and achieve path following of straight lines. Experimental results illustrated the performance of the proposed control strategy. In summary, the proposed integral LOS path following controller successfully steered the underwater snake robot towards and along the desired straight path, compensating the effects of currents. From the experimental results, it is seen that the robot managed to orient itself and maintain a constant non-zero heading to compensate for the effect of the current forces.

In future work, the authors will investigate the validity of the proposed control strategy for general path following control purposes and extend the proposed control approach by taking into account general disturbances that could affect the motion of the robot operating in a highly uncertain underwater environment. In particular, a topic of future work is the extension of the proposed control approach to 3D in order to be able to investigate path following of underwater snake robots in a 3D plane.

REFERENCES

[1] E. Kelasidi, K. Y. Pettersen, J. T. Gravdahl, and P. Liljebäck, "Modeling of underwater snake robots," in *Proc. IEEE International Conference on Robotics and Automation (ICRA)*, Hong Kong, China, May 31-June 7 2014, pp. 4540–4547.

[2] E. Kelasidi, K. Y. Pettersen, P. Liljebäck, and J. T. Gravdahl, "Integral line-of-sight for path-following of underwater snake robots," in *Proc. IEEE Multi-Conference on Systems and Control*, Juan Les Antibes, France, Oct. 8-10 2014, pp. 1078 – 1085.

[3] M. Kruusmaa, P. Fiorini, W. Megill, M. De Vittorio, O. Akanyeti, F. Visentin, L. Chambers, H. El Daou, M.-C. Fiazza, J. Jezov, M. Listak, L. Rossi, T. Salumae, G. Toming, R. Venturelli, D. Jung, J. Brown, F. Rizzi, A. Qualtieri, J. Maud, and A. Liszewski, "Filose for svenning: A flow sensing bioinspired robot," *IEEE Robotics Automation Magazine*, vol. 21, no. 3, pp. 51–62, 2014.

[4] E. Borhaug, A. Pavlov, and K. Pettersen, "Integral LOS control for path following of underactuated marine surface vessels in the presence of constant ocean currents," in *Proc. 47th IEEE Conference on Decision and Control (CDC)*, Cancun, Dec. 9-11 2008, pp. 4984–4991.

[5] W. Caharija, K. Pettersen, A. Sorensen, M. Candeloro, and J. Gravdahl, "Relative velocity control and integral line of sight for path following of autonomous surface vessels: Merging intuition with theory," *Part M: Journal of Engineering for the Maritime Environment*, vol. 228, no. 2, 2013.

[6] P. Liljebäck, Ø. Stavdahl, K. Pettersen, and J. Gravdahl, "Mamba - a waterproof snake robot with tactile sensing," in *Proc. International Conference on Intelligent Robots and Systems (IROS)*, Chicago, IL, Sept. 14-18 2014, pp. 294–301.

[7] K. McIsaac and J. Ostrowski, "Motion planning for anguilliform locomotion," *IEEE Transactions on Robotics and Automation*, vol. 19, no. 4, pp. 637–625, 2003.

[8] K. Morgansen, B. Triplett, and D. Klein, "Geometric methods for modeling and control of free-swimming fin-actuated underwater vehicles," *IEEE Transactions on Robotics*, vol. 23, no. 6, pp. 1184–1199, 2007.

[9] P. Liljebäck, K. Y. Pettersen, Ø. Stavdahl, and J. T. Gravdahl, *Snake Robots: Modelling, Mechatronics, and Control*. Springer-Verlag, Advances in Industrial Control, 2013.

[10] P. Liljebäck, K. Pettersen, O. Stavdahl, and J. Gravdahl, "Controllability and stability analysis of planar snake robot locomotion," *IEEE Transactions on Automatic Control*, vol. 56, no. 6, pp. 1365–1380, 2011.

[11] P. Liljebäck, K. Y. Pettersen, Ø. Stavdahl, and J. T. Gravdahl, "A review on modelling, implementation, and control of snake robots," *Robotics and Autonomous Systems*, vol. 60, no. 1, pp. 29–40, 2012.

[12] A. A. Transeth and K. Y. Pettersen, "Developments in snake robot modeling and locomotion," in *Proc. 9th International Conference on Control, Automation, Robotics and Vision (ICARCV)*, Singapore, Dec. 5-8 2006, pp. 1–8.

[13] J. Gray, "Studies in animal locomotion," *The Journal of Experimental Biology*, vol. 10, no. 1, pp. 88–104, 1933.

[14] S. Hirose, *Biologically Inspired Robots: Snake-Like Locomotors and Manipulators*. Oxford University Press, 1993.

[15] S. Hirose and H. Yamada, "Snake-like robots [tutorial]," *IEEE Robotics Automation Magazine*, vol. 16, no. 1, pp. 88–98, 2009.

[16] R. Crespi, A. Badertscher, A. Guignard, and A. J. Ijspeert, "Amphibot I: an amphibious snake-like robot," *Robotics and Autonomous Systems*, vol. 50, no. 4, pp. 163–175, 2005.

[17] C. Wright, A. Buchan, B. Brown, J. Geist, M. Schwerin, D. Rollinson, M. Tesch, and H. Choset, "Design and architecture of the unified modular snake robot," in *Proc. IEEE International Conference on Robotics and Automation (ICRA)*, May 2012, pp. 4347–4354.

[18] S. Ma, C. Ye, B. Li, and Y. Wang, "Reconfigurable modular universal unit (muu) for mobile robots," in *Distributed Autonomous Robotic Systems 8*, H. Asama, H. Kurokawa, J. Ota, and K. Sekiyama, Eds. Springer Berlin Heidelberg, 2009, pp. 453–461.

[19] P. Liljebäck, K. Y. Pettersen, and Ø. Stavdahl, "A snake robot with a contact force measurement system for obstacle-aided locomotion," in *Proc. IEEE International Conference on Robotics and Automation (ICRA)*, Anchorage, AK, USA, May 3-7 2010, pp. 683–690.

[20] K. Melsaac and J. Ostrowski, "A geometric approach to anguilliform locomotion: modelling of an underwater eel robot," in *Proc. International Conference on Robotics and Automation (ICRA)*, Detroit, MI, May 10-15 1999, pp. 2843–2848.

[21] K. McIsaac and J. Ostrowski, "Experiments in closed-loop control for an underwater eel-like robot," in *Proc. IEEE International Conference on Robotics and Automation (ICRA)*, Washington DC, May 12-18 2002, pp. 750–755.

[22] C. Wilbur, W. Vorus, Y. Cao, and S. Currie, *Neurotechnology for biomimetic robots, chapter A Lamprey-Based Undulatory Vehicle*, C. London, Ed. Bradford/MIT Press, 2002.

[23] A. Crespi and A. J. Ijspeert, "AmphiBot II: An Amphibious Snake Robot that Crawls and Swims using a Central Pattern Generator," in *Proc. 9th International Conference on Climbing and Walking Robots (CLAWAR)*, Brussels, Belgium, Sept. 2006, pp. 19–27.

[24] M. Porez, F. Boyer, and A. J. Ijspeert, "Improved lighthill fish swimming model for bio-inspired robots: Modeling, computational aspects and experimental comparisons," *The International Journal of Robotics Research*, vol. 33, no. 10, pp. 1322–1341, 2014.

[25] B. Li, S. Yu, S. Ma, and Y. Wang, "An amphibious snake-like robot with novel gaits on ground and in water," in *Proc. IASTED International Conference Intelligent Systems and Control (ISC 2011)*, Calgary, AB, July 11-13 2011, pp. 100–105.

[26] C. Ye, S. Ma, B. Li, and Y. Wang, "Locomotion control of a novel snake-like robot," in *Proc. IEEE/RSJ International Conference on Intelligent*

Robots and Systems (IROS), Sendai, Japan, Sept. 28-02 2004, pp. 925–930.

[27] H. Yamada, S. Chigisaki, M. Mori, K. Takita, K. Ogami, and S. Hirose, "Development of amphibious snake-like robot ACM-R5," in *Proc. 36th International Symposium on Robotics*, Tokyo, Japan, 2005.

[28] T. Takayama and S. Hirose, "Amphibious 3d active cord mechanism "helix" with helical swimming motion," in *Proc. IEEE/RSJ International Conference on Intelligent Robots and Systems (IROS)*, Lausanne, Switzerland, Sept. 30-Oct. 2 2002, pp. 775 – 780.

[29] C. Stefanini, S. Orofino, L. Manfredi, S. Mintchev, S. Marrazza, T. Assaf, L. Capantini, E. Sinibaldi, S. Grillner, P. Wallen, and P. Dario, "A novel autonomous, bioinspired swimming robot developed by neuroscientists and bioengineers," *Bioinspiration & Biomimetics*, vol. 7, no. 2, p. 025001, 2012.

[30] J. Liu, I. Dukes, and H. Hu, "Novel mechatronics design for a robotic fish," in *Proc. IEEE/RSJ International Conference on Intelligent Robots and Systems (IROS)*, Canada, Aug 2-6 2005, pp. 807–812.

[31] L. Wen, T. Wang, G. Wu, and J. Li, "A novel method based on a force-feedback technique for the hydrodynamic investigation of kinematic effects on robotic fish," in *Proc. IEEE International Conference on Robotics and Automation (ICRA)*, Shanghai, May 9-13 2011, pp. 203–208.

[32] D. J. Klein, P. K. Bettale, B. I. Triplett, and K. A. Morgansen, "Autonomous underwater multivehicle control with limited communication: Theory and experiment," *Proc. Second IFAC Workshop on Navigation, Guidance and Control of Underwater Vehicles*, vol. 2, no. 1, pp. 113–118, 2008.

[33] G. Taylor, "Analysis of the swimming of long and narrow animals," *Proc. Royal Society of London. Series A. Mathematical and Physical Sciences*, vol. 214, no. 1117, pp. 158–183, 1952.

[34] M. J. Lighthill, "Large-amplitude elongated-body theory of fish locomotion," *Proc. Royal Society of London. Series B. Biological Sciences*, vol. 179, no. 1055, pp. 125–138, 1971.

[35] F. Boyer, M. Porez, and W. Khalil, "Macro-continuous computed torque algorithm for a three-dimensional eel-like robot," *IEEE Transactions on Robotics*, vol. 22, no. 4, pp. 763 –775, 2006.

[36] J. Chen, W. O. Friesen, and T. Iwasaki, "Mechanisms underlying rhythmic locomotion: body-fluid interaction in undulatory swimming," *Journal of Experimental Biology*, vol. 214, no. 4, pp. 561–574, 2011.

[37] A. Wiens and M. Nahon, "Optimally efficient swimming in hyper-redundant mechanisms: control, design, and energy recovery," *Bioinspiration & Biomimetics*, vol. 7, no. 4, p. 046016, 2012.

[38] J. Blair and T. Iwasaki, "Optimal gaits for mechanical rectifier systems," *IEEE Transactions on Automatic Control*, vol. 56, no. 1, pp. 59–71, 2011.

[39] F. Candelier, M. Porez, and F. Boyer, "Note on the swimming of an elongated body in a non-uniform flow," *Journal of Fluid Mechanics*, vol. 716, pp. 616–637, 2013.

[40] L. Zhu, Z. Chen, and T. Iwasaki, "Oscillation, orientation, and locomotion of underactuated multilink mechanical systems," *IEEE Transactions on Control Systems Technology*, vol. 21, no. 5, pp. 1537–1548, 2013.

[41] T. McMillen and P. Holmes, "An elastic rod model for anguilliform swimming," *Journal of Mathematical Biology*, vol. 53, no. 5, pp. 843–886, 2006.

[42] G. Kosa, M. Shoham, and M. Zaaroor, "Propulsion method for swimming microrobots," *IEEE Transactions on Robotics*, vol. 23, no. 1, pp. 137–150, 2007.

[43] J. Colgate and K. Lynch, "Mechanics and control of swimming: A review," *IEEE Journal of Oceanic Engineering*, vol. 29, no. 3, pp. 660–673, 2004.

[44] J. Liu and H. Hu, "Biological inspiration: from carangiform fish to multi-joint robotic fish," *Journal of Bionic Engineering*, vol. 7, pp. 35–48, 2010.

[45] R. Clapham and H. Huosheng, "iSplash-II: realizing fast carangiform swimming to outperform a real fish," in *Proc. IEEE/RSJ International Conference on Intelligent Robots and Systems (IROS)*, Chicago, Illinois, Sept. 14-18 2014, pp. 1080–1086.

[46] D. Jung, P. Pott, T. Salumae, and M. Kruusmaa, "Flow-aided path following of an underwater robot," in *Proc. IEEE International Conference on Robotics and Automation (ICRA)*, Karlsruhe, Germany, May 6-10 2013, pp. 4602–4607.

[47] S. Bi, H. Ma, Y. Cai, C. Niu, and Y. Wang, "Dynamic modeling of a flexible oscillating pectoral fin for robotic fish," *Industrial Robot: An International Journal*, vol. 41, no. 5, pp. 421–428, 2014.

[48] A. Rasmussen, K. Sanders, M. Guinea, and A. Amey, "Sea snakes in australian waters (serpentes: subfamilies hydrophiinae and laticaudinae)-a review with an updated identification key." *Zootaxa*, vol. 3869, no. 4, pp. 351–71, 2014.

[49] F. Boyer, M. Porez, A. Leroyer, and M. Visonneau, "Fast dynamics of an eel-like robot-comparisons with navier-stokes simulations," *IEEE Transactions on Robotics*, vol. 24, no. 6, pp. 1274–1288, 2008.

[50] O. Ekeberg, "A combined neuronal and mechanical model of fish swimming," *Biological Cybernetics*, vol. 69, no. 5-6, pp. 363–374, 1993.

[51] W. Khalil, G. Gallot, and F. Boyer, "Dynamic modeling and simulation of a 3-D serial eel-like robot," *IEEE Transactions on Systems, Man, and Cybernetics, Part C: Applications and Reviews*, vol. 37, no. 6, pp. 1259–1268, 2007.

[52] E. Kelasidi, K. Pettersen, and J. Gravdahl, "Modeling of underwater snake robots moving in a vertical plane in 3D," in *Proc. IEEE/RSJ International Conference on Intelligent Robots and Systems (IROS)*, Chicago, Illinois, Sept. 14-18 2014, pp. 266–273.

[53] K. McIsaac and J. Ostrowski, "Open-loop verification of motion planning for an underwater eel-like robot," in *Experimental Robotics VII*, ser. Lecture Notes in Control and Information Sciences, D. Rus and S. Singh, Eds. Springer Berlin - Heidelberg, 2001, vol. 271, pp. 271–280.

[54] P. A. Vela, K. A. Morgansen, and J. W. Burdick, "Underwater locomotion from oscillatory shape deformations," in *Proc. 41st IEEE Conference on Decision and Control (CDC)*, Las Vegas, USA, Dec. 10-13 2002, pp. 2074–2080.

[55] K. McIsaac and J. Ostrowski, "A framework for steering dynamic robotic locomotion systems," *International Journal of Robotics Research*, vol. 22, no. 2, pp. 83–97, 2003.

[56] E. Kelasidi, K. Y. Pettersen, and J. T. Gravdahl, "A waypoint guidance strategy for underwater snake robots," in *Proc. IEEE 22nd Mediterranean Conference on Control and Automation*, Palermo, Italy, June 16-19 2014, pp. 1512–1519.

[57] J. Guo, "A waypoint-tracking controller for a biomimetic autonomous underwater vehicle," *Ocean Engineering*, vol. 33, no. 17-18, pp. 2369 – 2380, 2006.

[58] M. Porez, V. Lebastard, A. Ijspeert, and F. Boyer, "Multi-physics model of an electric fish-like robot: Numerical aspects and application to obstacle avoidance," in *Proc. IEEE/RSJ International Conference on Intelligent Robots and Systems (IROS)*, San Francisco, CA, Sept. 25-30 2011, pp. 1901–1906.

[59] M. Alamir, M. El Rafei, G. Hafidi, N. Marchand, M. Porez, and F. Boyer, "Feedback design for 3D movement of an eel-like robot," in *Proc. IEEE International Conference on Robotics and Automation (ICRA)*, Roma, Apr. 10-14 2007, pp. 256–261.

[60] M. El Rafei, M. Alamir, N. Marchand, M. Porez, and F. Boyer, "Motion control of a three-dimensional eel-like robot without pectoral fins," *Proc. 17th IFAC World Congress*, vol. 17, no. 1, pp. 750–755, 2008.

[61] ——, "Multi-variable constrained control approach for a three-dimensional eel-like robot," in *Proc. IEEE/RSJ International Conference on Intelligent Robots and Systems (IROS)*, Nice, France, Sept. 22-26 2008, pp. 3152–3157.

[62] L. Lapierre and B. Jouvencel, "Path following control for an eel-like robot," in *Proc. MTS/IEEE International Conference Oceans*, vol. 1, Brest, France, June 20-23 2005, pp. 460–465.

[63] E. Kelasidi, P. Liljebäck, K. Y. Pettersen, and J. T. Gravdahl, "Innovation in underwater robots: Biologically inspired swimming snake robots," *IEEE Robotics Automation Magazine*, vol. 23, no. 1, pp. 44–62, 2016.

[64] J. Bak-Coleman, A. Court, D. Paley, and S. Coombs, "The spatiotemporal dynamics of rheotactic behavior depends on flow speed and available sensory information," *The Journal of Experimental Biology*, vol. 216, no. 21, pp. 4011–4024, 2013.

[65] M. J. Kanter and S. Coombs, "Rheotaxis and prey detection in uniform currents by lake michigan mottled sculpin (cottus bairdi)," *The Journal of Experimental Biology*, vol. 206, no. 1, pp. 59–70, 2003.

[66] S. Fan and C. Woolsey, "Underwater vehicle control and estimation in nonuniform currents," in *Proc. American Control Conference (ACC)*, Washington, DC, June 17-19 2013, pp. 1400–1405.

[67] T. I. Fossen, *Handbook of Marine Craft Hydrodynamics and Motion Control*. John Wiley & Sons, Ltd, 2011.

[68] E. Kelasidi, P. Liljebäck, K. Y. Pettersen, and J. T. Gravdahl, "Experimental investigation of efficient locomotion of underwater snake robots for lateral undulation and eel-like motion patterns," *Robotics and Biomimetics*, vol. 2, no. 1, pp. 1–27, 2015.

[69] E. Kelasidi, K. Y. Pettersen, and J. T. Gravdahl, "Energy efficiency of underwater snake robot locomotion," in *Proc. 23th Mediterranean Conference on Control Automation (MED)*, Torremolinos, Spain, June 16-19 2015, pp. 1124 – 1131.

[70] E. Kelasidi and A. Tzes, "Serpentine motion control of snake robots for curvature and heading based trajectory - parameterization," in *Proc. IEEE 20th Mediterranean Conference on Control Automation (MED)*, Barcelona, Spain, July 3-6 2012, pp. 536–541.

[71] H. K. Khalil, *Nonlinear Systems*, 3rd ed. Prentice Hall, Ed., 2002.

[72] T. Parker and L. Chua, *Practical numerical algorithms for chaotic systems*. Berlin: Springer Verlag, 1989.

[73] E. Kelasidi, K. Y. Pettersen, and J. T. Gravdahl, "A control-oriented model of underwater snake robots," in *Proc. IEEE International Conference on Robotics and Biomimetics (ROBIO)*, Bali, Indonesia, Dec. 5-10 2014, pp. 753–760.

[74] Dragon skin high performance silicone rubber. [Online]. Available: http://www.smooth-on.com

[75] Sintef fisheries and aquaculture flume tank. [Online]. Available: http://www.sintef.no/home/Fisheries-and-Aquaculture/About-us/Laboratories/SINTEF-Fisheries-and-aquaculture-flume-tank/

[76] Qualisys, *Qualisys-Motion Capture Systems*, 2015, http://www.qualisys.com.

Jan Tommy Gravdahl received the Siv.ing and Dr.ing degrees in engineering cybernetics from the Norwegian University of Science and Technology (NTNU), Trondheim, Norway, in 1994 and 1998, respectively.

He became an Associate Professor in 2001 and then Professor in 2005 in the Department of Engineering Cybernetics, NTNU, where he also served as the Head of the Department in 2008-2009. In 2007-2008, he was a Visiting Professor at the Centre for Complex Dynamic Systems and Control, The University of Newcastle, Newcastle, Australia. He has published more than 200 international conference and journal papers. He is the author of Compressor Surge and Rotating Stall: Modeling and Control (Springer, 1999), coauthor of Modeling and Simulation for Automatic Control (Marine Cybernetics, 2002), coeditor of Group Coordination and Cooperative Control (Springer, 2006), and coauthor of Snake Robots: Modelling, Mechatronics, and Control (Springer, 2013). He is also a coauthor of Modeling and Control of Vehicle-Manipulator Systems (Springer, 2013). His current research interests include mathematical modeling and nonlinear control in general, modeling and control of turbomachinery, and control of vehicles, spacecraft, robots, and nanopositioning devices.

Prof. Gravdahl received the IEEE TRANSACTIONS ON CONTROL SYSTEMS TECHNOLOGY Outstanding Paper Award in 2000.

Eleni Kelasidi received the Diploma (MSc) of Electrical and Computer Engineering and the Ph.D degree in Engineering Cybernetics from the University of Patras, Greece, in 2009 and from Norwegian University of Science and Technology (NTNU), Trondheim, Norway, in 2015, respectively. In 2009-2012, she was a pre-doc researcher in the field of design and control of mobile robot with articulated body at the University of Patras. She is currently a PostDoc Researcher (VISTA Scholar) at the CoE Centre for Autonomous Marine Operations and Systems, Department of Engineering Cybernetics, NTNU. Her research interests include modeling, analysis and control of underwater snake robots.
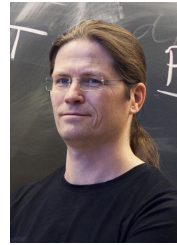
Pål Liljebäck received the M.Sc. and Ph.D. degrees in electrical engineering from the Norwegian University of Science and Technology (NTNU), Trondheim, Norway, in 2004 and 2011, respectively. He is currently an Innovation Researcher at the Department of Engineering Cybernetics, NTNU, and he is also the CTO of Eelume AS, a spin-off company from NTNU developing subsea robotics solutions. He was a Research Scientist at SINTEF ICT, Department of Applied Cybernetics, Trondheim, Norway, in the period 2004 - 2015. He is the author of Snake Robots: Modelling, Mechatronics, and Control (Springer, 2013). His research interests include modeling and control of dynamical systems, and design and implementation of mechatronic systems.

Kristin Y. Pettersen is a Professor in the Department of Engineering Cybernetics, NTNU where she has been a faculty member since 1996. She was Head of Department 2011-2013, Vice-Head of Department 2009-2011, and Director of the NTNU ICT Programme of Robotics 2010-2013. In the period 2013 - 2022 she is also Key Scientist at the CoE Centre for Autonomous Marine Operations and Systems (NTNU AMOS). She is CEO of the spin-off company Eelume AS.

She received the MSc and PhD degrees in Engineering Cybernetics at NTNU, Trondheim, Norway, in 1992 and 1996, respectively. She has published more than 200 international papers for conferences and journals, and her research interests focus on nonlinear control of mechanical systems with applications to robotics, with a special emphasis on marine robotics and snake robotics. She has served as a member of the Editorial Board of Simulation Modeling Practice and Theory, IEEE Transactions on Control Systems Technology and IEEE Control Systems Magazine. She was a member of the Board of Governors of IEEE Control Systems Society 2012 - 2014, and she has also held several board positions in industrial and research companies.